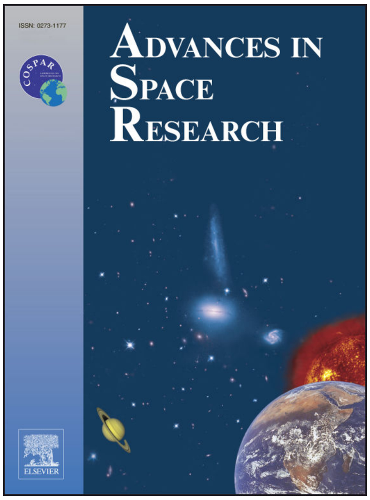

Dynamic GPS-based LEO orbit determination with 1 cm precision using the Bernese GNSS Software

Xinyuan Mao, Daniel Arnold, Valère Girardin, Arturo Villiger, Adrian Jäggi

PII: S0273-1177(20)30723-7
DOI: https://doi.org/10.1016/j.asr.2020.10.012
Reference: JASR 15010

To appear in: *Advances in Space Research*

Received Date: 10 July 2020
Revised Date: 1 October 2020
Accepted Date: 8 October 2020

Please cite this article as: Mao, X., Arnold, D., Girardin, V., Villiger, A., Jäggi, A., Dynamic GPS-based LEO orbit determination with 1 cm precision using the Bernese GNSS Software, *Advances in Space Research* (2020), doi: https://doi.org/10.1016/j.asr.2020.10.012

Dynamic GPS-based LEO orbit determination with 1 cm precision using the Bernese GNSS Software

Xinyuan Mao[a,*], Daniel Arnold[a], Valère Girardin[a,b], Arturo Villiger[a], Adrian Jäggi[a]

[a] *Astronomical Institute, University of Bern, Switzerland*
[b] *Now at: The Space Transportation Directorate of the European Space Agency, Paris, France*

Abstract

The Astronomical Institute of the University of Bern (AIUB) has been performing GPS-based Precise Orbit Determination (POD) for a large variety of Low Earth Orbit (LEO) satellites since two decades. Traditionally, LEO orbits have been generated by a reduced-dynamic POD strategy using the Bernese GNSS Software, replacing an explicit modeling of non-gravitational forces by dedicated empirical orbit parametrizations. This LEO POD strategy can be advanced by two main developments: on the one hand, use is made of the GNSS Observation-Specific Bias (OSB) and clock products provided by the Center for Orbit Determination in Europe (CODE), allowing for the resolution of single-receiver GNSS carrier-phase ambiguities. On the other hand, the main focus of this article, a refined satellite non-gravitational force modeling strategy is constructed to reduce the amount of empirical parameters used to compensate for force modeling deficiencies. LEO POD is first performed for Sentinel-3, a satellite formation currently consists of two identical satellites -3A and -3B, which experience a similar in-flight environment and allow for direct POD performance comparisons. A third satellite Swarm-C, which flies at a lower altitude and has a more sophisticated surface geometry, is selected to validate the robustness of the new POD strategy. As a result, both the internal consistency checks and

---

[*] Corresponding author; Tel.: +41 (0)31 631 3802
Email address: `xinyuan.mao@aiub.unibe.ch` (Xinyuan Mao)

external orbit validations suggest superior orbit quality obtained for the three satellites for a time span of 1.5 years (7 June, 2018 to 31 December, 2019). The ambiguity resolution adds strong constraints to the orbits and the satellite non-gravitational force modeling leads to more tightly constrained (towards zero) pseudo-stochastic empirical parameters. The final orbit solutions agree with external orbit solutions and independent satellite laser ranging measurements at levels of sub-cm, indicating approximately 20% improvement w.r.t. the nominal reduced-dynamic orbit solutions. This suggests potential benefits to the space geodesy community that always pursues best-possible satellite orbits.

Keywords: Precise Orbit Determination, Sentinel Satellites, Bernese GNSS Software, Non-gravitational Forces, Single-receiver Ambiguity Resolution

---

1. Introduction

Low Earth Orbit (LEO) satellites have significantly broadened our space exploration eyesight by successfully fulfilling various designated scientific tasks during the past years. They often necessitate Precise Orbit Determination (POD) products and many investigations have proven the GPS-based POD strategy as an inherent solution (Yunck, 1996). Since the late 80s, the Astronomical Institute of the University of Bern (AIUB) has been permanently developing and improving the Bernese GNSS Software (BSW), which is a scientific, high-precision, multi-GNSS and Satellite Laser Ranging (SLR) data processing software serving not only for practical applications, but also for space geodetic research, e.g., the International GNSS Service's (IGS) associated operational processing ~~(Beutler et al., 1987; Dach et al., 2015)~~ (Beutler et al., 1987; Dach et al., 2015; Johnston et al., 2017). Besides that, BSW was expanded to process LEO satellite data and has been proven successful in generating high-precision orbit solutions for several dedicated LEO Earth observation satellites (Jäggi et al., 2006; Bock et al., 2011; Jäggi et al., 2013; Arnold et al., 2019).

The preliminary motivation of this article is to improve the BSW orbit solutions for the European ~~Space Agency's (ESA) Sentinel series Earth observation~~ Sentinel satellites, in particular, for the Sentinel-3 satellites~~(Fernández et al., 2016).~~ . Sentinel is a constellation of Earth observation satellites primarily designed to provide long-term routine multidisciplinary observations for advancing Earth System sciences. Most of the onboard instrument systems are operating with different spectral bands and high spatial resolutions, which necessitate high-precision science orbits (Berger et al., 2012) . AIUB is a member of the Copernicus Precise Orbit Determination (CPOD) Quality Working Group (QWG), which is performing routine POD for the associated Sentinel satellites. The generated orbit solutions are supposed to monitor the performance of the operational CPOD ~~products~~ orbit products every four months through a so-called Copernicus POD Regular Service Review (RSR) project and to propose potential orbit enhancements through inter-agency comparisons ~~(Fernández et al., 2015; Fernández, 2019a)~~ (Fernández et al., 2015, 2019). Based on the experience in the ~~Regular Service Review (RSR)~~ RSR for the different Sentinel satellites, we realize that special attention needs to be paid to the POD of the Sentinel-3 mission, which is a satellite formation devoted to long-term oceanography, land-vegetation monitoring, and topographic mapping through radar altimetry~~(Fernández et al., 2016)~~ , etc. To meet with the prime scientific requirements, each Sentinel-3 satellite is equipped with a package of advanced payloads demanding precise orbits particularly in radial direction, where a precision of 3 cm should be achieved for the Non-Time Critical (NTC) applications and a precision of 2 cm after some days of post-facto POD refinement (Fernández et al., 2016). Its onboard dual-frequency high-precision 8-channel GPS receivers can be used for POD and the Laser Retro-Reflector (LRR) allows for external and independent orbit validations. Currently two identical Sentinel-3 satellites, -3A (launched on 16 February, 2016) and -3B (launched on 25 April, 2018) are flying in the same near-circular sun-synchronous orbit with an altitude of about 800 km.

Thanks to the decent coordination of the European Union's Copernicus Programme and the close collaborations among all QWG members, many LEO

POD advances are proposed and continuously improved Sentinel-3 orbits are generated. Peter et al. (2017, 2020) suggested corrections to the Antenna Reference Point (ARP) and/or Phase Center Offset (PCO) of the Sentinel GPS receivers. Hackel (2019) suggested a refined satellite non-gravitational force modeling strategy, which supported further investigation into the so-called single-receiver Integer Ambiguity Resolution (IAR) done by (Montenbruck et al., 2018a). More importantly, Montenbruck et al. (2018a) proposed a refined strategy for the generation of the GPS carrier-phase measurements of the Sentinel-3 GPS receiver that allows to avoid half-cycle ambiguities in the GPS data that have inhibited ambiguity-fixing before. This was also applied to the Swarm GPS receivers and proven to be rather successful in generating better absolute and relative orbits (Montenbruck et al., 2018b; Mao et al., 2018). Furthermore, they concluded a cross-track offset correction to the Center-of-Mass (CoM) of the Sentinel-3A satellite. This correction was officially accepted to change the GPS ARP (Fernández, 2019a). Kobel et al. (2019) took advantage of the Variance Component Estimation (VCE) of QWG's orbit products, obtaining a superior precision. Molina et al. (2019) evaluated the GPS L2C tracking performance of the Sentinel-3B GPS receiver and compared it with that of the Sentinel-3A satellite during their so-called *tandem phase*. These methodology improvements will be beneficial to a broader LEO POD community.

To fulfill our motivations, this article outlines and evaluates the two main LEO POD advances in BSW, which is modified to generate better orbit solutions for not only the Sentinel-3 mission, but also other LEO satellite missions. The major improvements for the LEO POD are the single-receiver IAR and the non-gravitational force modeling, which is the focus of this article.

On the one hand, use is made of the GNSS Observation-Specific Bias (OSB) and ambiguity fixed clock products provided by the Center for Orbit Determination in Europe (CODE), allowing for the single-receiver IAR (Schaer et al., 2020). The CODE products differ from not only the dedicated GPS orbit, clock and wide-lane bias products provided by the Centre National D'Études Spatiales/Collecte Localisation Satellites (CNES/CLS) (Loyer et al., 2012; Montenbruck et al., 2018a), but also the phase bias products generated at the Jet Propulsion Laboratory (JPL) (Bertiger et al., 2010)~~, It~~. However, it has to be noted that this article does not introduce the implemented single-receiver IAR algorithm, which will be elaborated by ~~Schaer et al. (2020); ?~~ Schaer et al. (2020).

On the other hand, a refined satellite non-gravitational force modeling strategy is proposed and implemented for the Sentinel-3 satellites and the Swarm-C satellite, which is a component satellite of the ESA's geomagnetic field mission Swarm (Friis-Christensen et al., 2008). The modeling consists of comprehensive modeling of Solar Radiation Pressure (SRP), Earth Radiation Pressure (ERP) and Aerodynamic Force (AF) acting on the surfaces of a satellite. We use a description of the Sentinel-3 satellites in terms of an 8-plate macro-model (Fernández, 2019a), whereas the Swarm satellite geometry is modeled as a more complex 15-plate macro-model (Montenbruck et al., 2018b). SRP and ERP are modeled considering spontaneous re-emission on non-solar plates (Ries et al., 1993; Cerri et al., 2010). Besides, a linear interpolation between monthly Clouds and the Earth's Radiant Energy System (CERES) S4 grid products is specifically done for the ERP modeling (Wielicki et al., 1996). This differs from Hackel (2019) who makes use of groups of polynomial coefficients to represent these grids. In addition, arc-specific scale factors for SRP and AF are co-estimated to compromise with the potential mis-modeling of non-gravitational forces.

POD for three LEO satellites are investigated to check the performance of the dynamic orbit modeling strategies. A common period, from 7 June, 2018 to 31 December, 2019, is selected for all satellite data processing. The two Sentinel-3 satellites have always been flying in the same orbit plane, guaranteeing a nearly identical in-flight perturbation environment. The Swarm-C satellite was flying at an altitude of about 500 km (Friis-Christensen et al., 2008), which was roughly 300 km lower than the Sentinel-3 satellites. Such an altitude is supposed to cause significantly stronger AF acting on a satellite due to a larger neutral atmospheric density (Doornbos, 2012). The Swarm-C POD acts as a more challenging scenario to validate the POD strategy comprehensively.

This article is organized as follows. Sect.2 introduces the different POD strategies implemented in BSW. As the backbone of our research, the detailed non-gravitational force modeling strategy is outlined in Sect.3. Sect.4 analyzes and discusses the different orbit solutions. They are checked internally and validated externally using independent orbit solutions from other institutions and also SLR measurements. Finally, Sect.5 concludes this article and gives a general outlook.

2. Precise Orbit Determinations in BSW

This section introduces the 6 different POD orbit solutions (Tab.1) that can be generated by BSW. The new features of the proposed non-gravitational force modeling POD strategy will be elaborated subsequently.

Firstly, a kinematic POD strategy is fully independent of LEO satellite force models. A kinematic orbit is an ephemeris at discrete measurement epochs since all positions are determined solely from a high-low satellite-to-satellite geometric positioning. Therefore it requires a minimum number (normally ≥ 5 to guarantee redundancy) of tracked GPS satellites for solving four unknown parameters (3 coordinates and 1 clock offset) of a receiver. The kinematic orbit quality is heavily dependent on the performance of GPS receivers and no solutions are available for epochs experiencing large data outliers or gaps (Yunck, 1996). In BSW, a typical kinematic orbit in the Earth-Centered Inertial (ECI) reference system is related to an epoch-wise trajectory of the antenna phase center position $\vec{r}_{leo}$, which is modeled as

$$\vec{r}_{leo}(t_{leo}) = \mathbf{R}(t_{leo}) \cdot (\vec{r}_{leo,e,0}(t_{leo}) + \delta\vec{r}_{leo,e,ant}(t_{leo})) \tag{1}$$

where $\vec{r}_{leo,e,0}$ is the CoM of a LEO satellite in the Earth-Centered Earth-Fixed (ECEF) reference frame, $\mathbf{R}$ denotes a transformation matrix from the ECEF to ECI reference frame. $\delta\vec{r}_{leo,e,ant}$, defined in the above equation, also in the ECEF reference frame, is GPS receiver antenna offset vector from CoM. Besides the geometry offset of ARP it also includes frequency-dependent antenna PCO and

Phase Center Variation (PCV) that can be created through ground experiments, or currently through a ~~*Residual Approach*~~*residual approach* using the in-flight GPS data (Jäggi et al., 2009). A typical scientific application of a kinematic trajectory is gravity field recovery from data of non-dedicated gravity missions ~~(??)~~(Jäggi et al., 2016; Teixeira da Encarnação et al., 2020).

Secondly, contrary to a pure kinematic orbit, a dynamic orbit is a particular solution fully dependent on the equation of motion and the underlying force models, e.g. the Earth gravity field. A typical representation of a dynamic orbit described in the ECI reference system and its initial conditions can be given by

$$
\begin{aligned}
\vec{r}_{leo}(t_{leo}) &= \vec{r}_{leo,0}(t_{leo}; a, e, i, \Omega, \omega, u_0; Q_1, ..., Q_d) + \delta\vec{r}_{leo,ant}(t_{leo}) \\
\ddot{\vec{r}} &= -GM\frac{\vec{r}}{r^3} + \vec{f}(t, \vec{r}, \dot{\vec{r}}, Q_1, ..., Q_d) \\
\vec{r}(t_0) &= \vec{r}(a, e, i, \Omega, \omega, u_0; t_0) \\
\dot{\vec{r}}(t_0) &= \dot{\vec{r}}(a, e, i, \Omega, \omega, u_0; t_0)
\end{aligned}
\tag{2}
$$

note that here $\vec{r}_{leo,0}$ denotes the LEO CoM coordinate in the ECI frame, $a, e, i, \Omega, \omega, u_0$ are the six osculating Keplarian elements of the orbit at t_0, GM is the gravitational constant times mass of the Earth, $Q_1, ..., Q_d$ indicate d empirical parameters used to compensate for force modeling deficiencies. This satellite trajectory can be described by a particular solution of the equation of motions w.r.t. satellite force models and empirical parameters Q, e.g. co-estimated parameters that are scaling dynamic force models. It is difficult to determine an ideal dynamic orbit for a LEO satellite which orbits the Earth in such a heavily perturbed environment that perturbations might vary significantly even in a short orbit arc.

Lastly, a reduced-dynamic orbit is a comprehensive trade-off between the kinematic and dynamic solutions, taking the advantages of both. The strength of force models can be reduced by including additional empirical parameters, e.g. the so-called pseudo-stochastic parameters (Jäggi et al., 2006). Normally for LEO satellite data processing in BSW, these are framed as a pre-defined number of Piece-wise Constant Accelerations (PCAs) to ensure that a satellite trajectory is continuous and differentiable at any epoch. PCAs can be first characterized by a priori known statistical properties, e.g. a priori variances σ_p^2 and spacing time Δ_t. The equation of motion of a reduced-dynamic orbit in the ECI reference frame can be represented by

$$\ddot{\vec{r}} = -GM\frac{\vec{r}}{r^3} + \vec{f}(t, \vec{r}, \dot{\vec{r}}, Q_1, ..., Q_d, P_1, ..., P_s) \tag{3}$$

where, compared with Eq. 2 and given the same initial conditions, $Q_1, ..., Q_d$ are often set as periodic and/or once-per-arc constant accelerations in three directions defined by the local orbital reference frame (i.e. radial, along-track and cross-track directions). $P_1, ..., P_s$ are the s pseudo-stochastic parameters to compensate for force modeling deficiencies. BSW was traditionally used without explicit modeling of non-gravitational forces, a reduced-dynamic POD approach which was very successful to generate LEO orbit solutions of high quality, e.g. (Jäggi et al., 2007; Bock et al., 2011). It required, however, relatively loose constraints to fully compensate for the not explicitly modeled non-gravitational forces with PCAs, which are usually set up over intervals ranging from about 5 to 15 minutes (Jäggi et al., 2006). Thanks to the new non-gravitational force modeling capabilities, the uncertainties of satellite dynamics are significantly reduced, which may lead to more tightly constrained (towards zero) pseudo-stochastic parameters. Especially when it comes to a reliable radial leveling e.g. for altimetry satellites, the use of empirical and pseudo-stochastic parameters should be carefully revised/limited, since they will allow to degrade the orbit if offset problems of any kinds (e.g. PCO and CoM) exist.

Therefore in our research, advances are made in the explicit modeling of non-gravitational forces and reducing the heavy dependence on empirical parameters, suggesting a more *dynamic* orbit solution. It will be shown that once-per-arc constant accelerations can be removed and PCAs can be more ~~more~~ tightly constrained towards zero, i.e. the a priori standard deviation (STD) σ_p is reduced by a factor of 10 specifically for the associated satellites in this article.

An overview of the new satellite dynamic modeling and POD processing strategy is summarized in Tab.2. Details for each non-gravitational force modeling will be elaborated in Sect. 3.

Table 1: Three LEO POD solutions - kinematic (KN), nominal (NM) reduced-dynamic, reduced-dynamic with non-gravitational force modeling (NG) - are computed. Single-receiver ambiguities can be either fixed to integers (IA) or remain float (FA). The 3-dimensional PCAs settings for the Sentinel-3 and Swarm-C satellites are different.

Sol.	IAR	Ngrv	Const. acc.	PCA (~~σ_p, $\Delta t = 360\ s$,~~ $\Delta t = 360\ s$, σ_p nm/s^2)
FAKN	No	No	No	No
FANM	No	No	Yes	Yes (5.0 or 10.0)
FANG	No	Yes	No	Yes (0.5 or 1.0)
IAKN	Yes	No	No	No
IANM	Yes	No	Yes	Yes (5.0 or 10.0)
IANG	Yes	Yes	No	Yes (0.5 or 1.0)

Six orbit solutions are generated for each satellite according to Tab.1. A nominal (NM) solution is a standard BSW reduced-dynamic solution without non-gravitational force modeling, all satellite dynamic mis-modelings are supposed to be absorbed by the once-per-arc constant accelerations and PCAs that necessitate more relaxed constraints (Jäggi et al., 2006). In this article, 240 groups of PCAs aligned in three directions (720 parameters) are evenly spaced and estimated for a 24-h orbit arc. Modeling each non-gravitational force (NG) allows us to tightly constrain the constant accelerations and PCAs towards zero. The a priori STD set up of PCAs for the Swarm-C satellite will be doubled as compared to the Sentinel-3 satellites due to stronger perturbations. A kinematic (KN) orbit serves as reference for internal consistency checks. All orbit solutions are computed using either fixed integer ambiguities (IA) or float ambiguities (FA). Please note that in BSW the carrier-phase integer ambiguities are resolved based on the OSB and clock products provided by CODE (Dach et al., 2019; Arnold et al., 2018; Schaer et al., 2020).

Table 2: Overview of force models, data processing and important parameterization in BSW. The associated information regarding the newly implemented non-gravitational force models is marked in blue.

Satellite information	Sentinel-3: 8-plate macro-model (Fernández, 2019a)
	Swarm-C: 15-plate macro-model (Montenbruck et al., 2018b)
	Internally processed Sentinel-3A PCV patterns: 253 days of time interval (DOY) 2016/054-2016/335
	Internally processed Sentinel-3B PCV patterns: 36 days of time interval 2018/121-2018/167
	Internally processed Swarm-C PCV patterns: 121 days of time interval 2015/152-2015/273
	Recommended PCO corrections to the Sentinel GPS antennas (Peter et al., 2017)
	1 cm correction to the Sentinel-3A CoM in +Y direction (Montenbruck et al., 2018a)
	Official mass table, quaternion attitude and instrument reference points, etc.
Earth parameters	Leap seconds table of TAI-UTC
	CODE Earth rotation parameters (Dach et al., 2019)
	Earth IERS2010XY sub-daily pole model and IAU2000R06 nutation model (Dach et al., 2015)
	Earth FES2004 ocean and Ray/Ponte barometric tides and CoM correction (Ray and Ponte, 2003; Lyard et al., 2006)
Gravitational forces	Earth GOCO05S 120×120 static gravity field (Mayer-Gürr et al., 2015)
	N-body planetary perturbations based on the JPL DE405 ephemerides (Standish et al., 1992)
	Earth solid tidal potential model TIDE2000 (Dehant et al., 1999)
	EOT11A 50×50 empirical ocean tide model (Savcenko and Bosch, 2012)
Aerodynamic force	Plate-wise lift and drag (Doornbos, 2012; Girardin, 2016)
	DTM-2013 atmospheric density model (Bruinsma, 2015)
	HWM-14 horizontal wind model (Drob et al., 2015)
	Goodman accommodation coefficients (Doornbos, 2012)
	Estimated scale factor
Solar radiation pressure	Plate-wise radiation pressure and spontaneous re-emission for non-solar plates (Cerri et al., 2010)
	Conical Earth and Moon shadows
	Radiation pressure coefficients (Doornbos, 2012)
	~~Scale~~ Estimated scale factor
Earth radiation pressure	Plate-wise reflectivity and emissivity, and spontaneous re-emission for non-solar plates (Hackel, 2019)
	Radiation pressure coefficients (Doornbos, 2012)
	Averaged monthly grids processed using CERES-S4 data (Wielicki et al., 1996)
	Linear interpolation between neighboring monthly grids
Arc-wise const. acc.	Only set for nominal reduced-dynamic POD
Piece-wise const. acc.	Sentinel-3: $\Delta t = 360\ s$, σ_p =0.5 nm/s^2 (×10 for nominal reduced-dynamic POD)
	Swarm-C: $\Delta t = 360\ s$, σ_p =1 nm/s^2 (×10 for nominal reduced-dynamic POD)
GPS products	CODE GPS orbits and 5s clock corrections (Dach et al., 2019)
	IGS14.atx GPS transmitter antenna PCO and PCV from IGS (Schmid et al., 2016)
	CODE GNSS Observation-Specific Bias products ~~(Schaer et al., 2020)~~ (Arnold et al., 2018; Schaer et al., 2020)
GPS data editing	Elevation cut-off: ~~0 deg~~0°, all GPS observations are used for data screening
	Observations for POD: carrier-phase only, ionosphere-free combination (Dach et al., 2015)
	Carrier-phase editing threshold: 4 cm
Orbit arc length	24 h
Data sampling	10 s
Ambiguity property	Single-receiver float ambiguity (no IAR) or integer ambiguity (IAR)

3. Non-gravitational Force Modeling

A LEO satellite normally experiences more complex perturbations than satellites at higher altitudes. The main perturbations are gravitational forces that can be numerically computed based on various supporting models (Tab.2). The modeling of non-gravitational forces is more challenging since it often relies on various external products which unfortunately can not perfectly represent the real in-flight perturbation environment (Doornbos, 2012). Therefore more empirical parameters are necessitated to address the model imperfections, and often the co-estimation of dimensionless scale factors during a POD process is conducted to absorb deficiencies of modeled forces and satellite macro-model. In this article, only SRP and AF are scaled, the ERP is not scaled since it will impact the orbit leveling particularly in radial direction (Montenbruck et al., 2018a; Hackel, 2019). The overall non-gravitational forces can be given by

$$\vec{f}_{Ngrv} = S_{SRP}\vec{f}_{SRP} + \vec{f}_{REF} + \vec{f}_{EMT} + S_{AF}\vec{f}_{AF} \tag{4}$$

where SRP, the Earth REFlectivity radiation pressure (REF), the Earth EMissiviTy radiation pressure (EMT) and AF are the surface forces considered. As stated above, a description of LEO satellites in terms of flat-plate macro-models is widely accepted for non-gravitational force modeling. This article uses the Sentinel-3 8-plate macro-model introduced in (Fernández, 2019a), which has been widely used by the CPOD and QWG community. The Swarm-C satellite has a more lengthy complex geometry, which can be described by a 15-plate macro-model (Montenbruck et al., 2018b; Hackel, 2019). In this article, self-shadowing effects are not addressed and each plate is treated independently. Peter et al. (2020) did a preliminary research of the self-shadowing effect for the Sentinel-1 satellites, however no relevant investigations were done to the Sentinel-3 and ~~the other LEO~~ Swarm satellites (Hackel, 2019; Van den IJssel et al., 2020; Vielberg and Kusche, 2020).

3.1. Solar Radiation Pressure

SRP originates from the interaction between photons and satellite surface materials. In general it can be divided into three categories - absorption, specular reflection and diffuse reflection - which are determined by the characteristics of surface materials. SRP is causing an acceleration given by

$$\vec{f}_{SRP} = \sum_{i=1}^{n} \frac{\vec{C}_{S,i}}{m} \left(\frac{1AU}{r_{Sun,s}} \right)^2 f_s P_{1AU} \tag{5}$$

where the index i enumerates all plates of the macro-model, the satellite mass m can be extracted from an official mass table, P_{1AU} is the solar radiation pressure at the distance of 1 AU (astronomical unit), $r_{Sun,s}$ is the distance between the Sun and the satellite, and f_s denotes the so-called geometric shadowing factor which takes into account a few impacting factors e.g. the proportions of Sun radiation absorbed by the atmosphere, eclipse, satellite and Earth shadowing, etc. (Doornbos, 2012; Hackel et al., 2017). The focus of computing SRP is modeling $\vec{C}_{S,i}$, a vectorial radiation pressure coefficient for a certain plate i. It is given by Doornbos (2012); Montenbruck and Gill (2012) (note Eq. 6 removes i for the sake of readability)

$$\begin{aligned} \vec{C}_S &= p_d \vec{C}_{S,d} + p_s \vec{C}_{S,s} + p_a \vec{C}_{S,a} \\ \vec{C}_{S,d} &= (\vec{r}_{Sun,s} - \frac{2}{3}\vec{n}) A\gamma \\ \vec{C}_{S,s} &= -2\gamma \vec{n} A\gamma \\ \vec{C}_{S,a} &= \vec{r}_{Sun,s} A\gamma - \frac{2}{3}\vec{n} A\gamma \end{aligned} \tag{6}$$

where, the fractions of diffuse reflection (p_d), specular reflection (p_s), and absorption (p_a) of photons for the short-wavelength visible radiation are described by the macro-model and they sum to 1. $\vec{n}$ denotes the unit vector of a plate's surface normal that usually points outwards, A is the surface area of the plate, $\gamma = -\vec{r}_{Sun,s} \cdot \vec{n}$ is the negative dot product of the plate's normal vector and the vector pointing from the Sun to the satellite. Absorbed photons will transfer all momentum to the satellite, and if no actions are done, e.g. the solar arrays generate power, the accumulation of energy will increase the temperatures of particularly non-solar plates. Normally, spacecraft engineers are aiming for a thermal balance and protect these plates with special materials such as polyimide. Therefore, we assume that all the absorbed photons will be spontaneously re-emitted according to Lambert's cosine law, as marked by the blue term of Eq. 6, according to the formula it is then exactly the same with $\vec{C}_{S,d}$ (Cerri et al., 2010; Hackel et al., 2017).

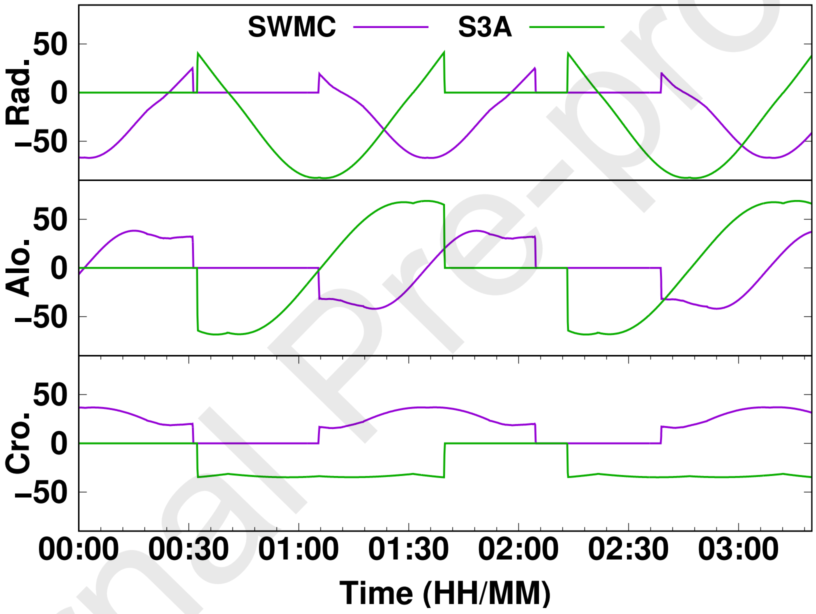

Figure 1: SRP modeling comparison between the Swarm-C and Sentinel-3A satellites (no scale factors applied). Selected period: 7 June, 2018 (DOY:158) 00:00-03:20, roughly two orbits for the Sentinel-3A satellite. Unit: $[nm/s^2]$.

A short-term (200 mins) comparison between the modeled SRPs for the Sentinel-3A and Swarm-C satellites is displayed in Fig.1. In general, the Sentinel-3A satellite experiences stronger SRP mainly due to its larger solar arrays of an area of 10.5 m^2, as compared to 3.45 m^2 for the Swarm-C satellite. The different signs in cross-track direction are caused by the different beta angles, i.e. elevations of the Sun above satellite orbital planes. For the selected orbit arc the Sentinel-3A satellite's beta angle is 23.2° and that for the Swarm-C satellite is $-28.5°$. In fact, the Sentinel-3 formation has quite stable beta angles only ranging between 23.2° and 34.5° during the 1.5 years due to its Sun-synchronous orbit (inclination 98.6°), whereas the Swarm-C satellite's beta angles vary from $-79.4°$ to 81.2° due to its more polar orbit (inclination 87.4°). Variations of the beta angles are visible in Fig.9.

3.2. Earth Radiation Pressure

The Earth's energy budget accounts for a balanced situation where the Earth reflects and emits nearly all incoming solar radiation back into the outer space. ERP is caused by 1) scattered short-wavelength visible solar radiation and 2) emitted long-wavelength thermal infrared radiation of the Earth. A few scientific satellites such as NASA's Aqua and Terra, have been continuously measuring the radiosity of the Earth. In BSW the monthly Clouds and the Earth's Radiant Energy System (CERES) S4 grid products, obtained from the Aqua and Terra satellites with a spatial resolution of $2.5° \times 2.5°$, are used to compute the corresponding ratios of radiative flux to the incoming solar irradiance, which is set to 1372 W/m^2 at 1 AU (Wielicki et al., 1996). In the work done by Hackel et al. (2017); Montenbruck et al. (2018b), the CERES-S4 grids were represented by zonal coefficients of Legendre polynomials to compromise between computation efficiency and modeling accuracy. Please note that there are different types of CERES associated products, e.g. Vielberg and Kusche (2020) made use of the CERES hourly SYN1deg data for a more refined modeling ERP.

All possible monthly CERES-S4 data from July 2002 to September 2019 are retrieved to generate the reflectivity and emissivity grids. The variations of the mean of monthly grids are displayed in Fig.2. It reveals that both reflectivity and emissivity grids change significantly from month to month, nevertheless they are rather stable for the same month from year to year, within a difference of merely 0.01. It is also interesting to see that the reflectivity has been decreasing during the past years. During the selected period, there are four months (August 2002, January 2011, December 2011, and August 2014) affected by

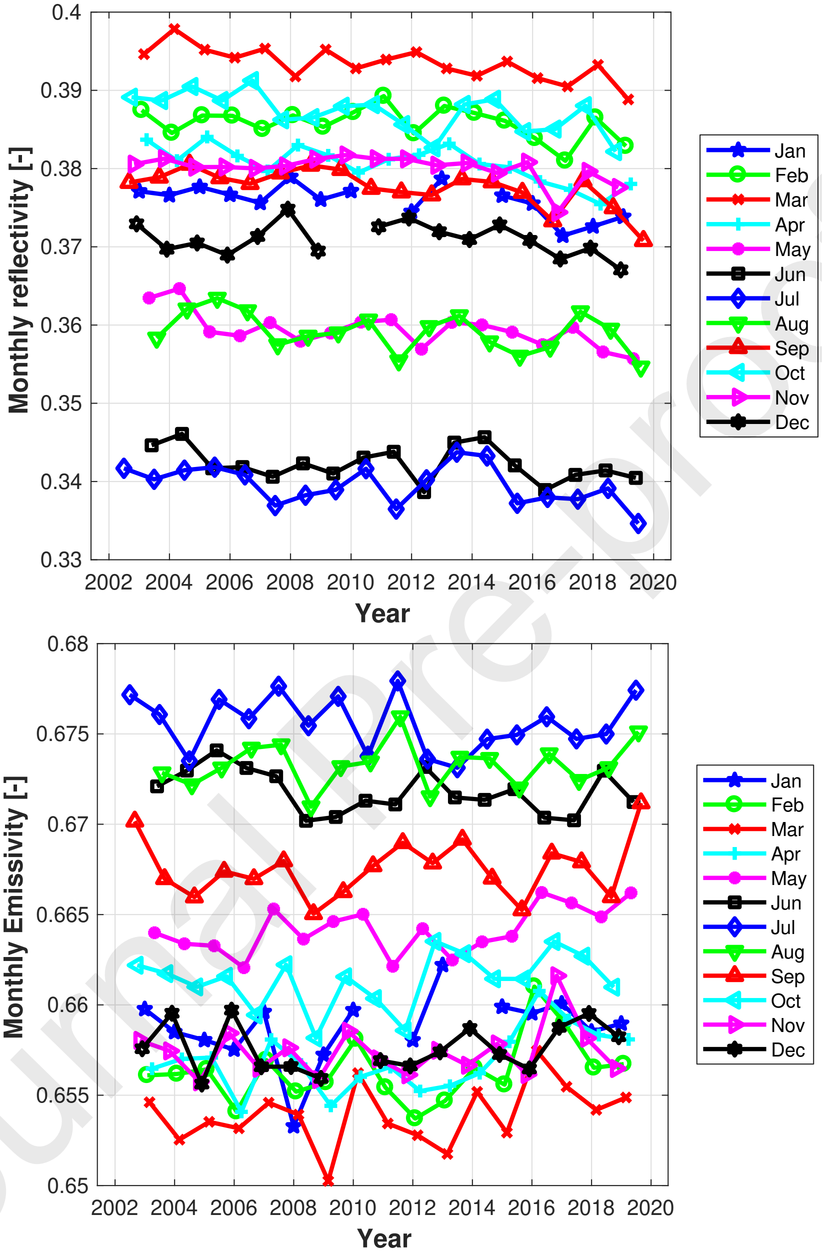

Figure 2: Variations of the mean of the monthly Earth reflectivity (top) and emissivity (bottom) radiation pressure grids, processed based on the CERES-S4 data from July 2002 to September 2019.

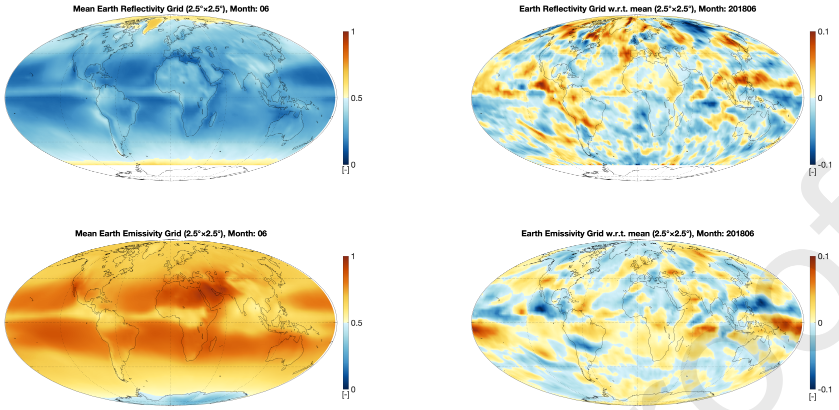

Figure 3: Left: the averaged Earth reflectivity (top) and emissivity (bottom) grids for June computed based on the CERES-S4 data between July 2002 and September 2019; Right: the difference between June 2018 grids and the averaged June grids. Figures are created using scripts shared in (Bezděk et al., 2013). Please note that different color bar limits are used from left to right.

data gaps. The CERES-S4 products also have a latency of a few months, which might obstruct a near-real-time POD processing, e.g., for the Sentinel RSR ~~(Fernández, 2019a)~~(Fernández et al., 2019). To overcome these deficiencies, we average the monthly products from all available years. The averaged grid for June, and the difference between the averaged and the specific June 2018 grid, are depicted in Fig.3. The seasonal reflectivity and emissivity changes are visible particularly for the high-latitude regions during the polar nights and days. In addition, an averaged monthly grid can not fully describe the dynamic variation within a month, therefore a linear interpolation is performed between the current monthly grid and its neighboring monthly grid, which is selected as either the previous month or the next month depending on the day of month for orbit computation. When comparing with the ERP modeling for the Sentinel-3A satellite using the specific monthly grid e.g. for June 2018, the modeled forces using the averaged June grid and performing the additional linear interpolation between two months (May and June) show discrepancies at levels within 1% (selected period: 7 June, 2018, 00:00-03:20, consistent with Fig.4), which can be easily handled by PCAs and do not impact the reduced-dynamic LEO POD solutions at a visible manner. Therefore we use the averaged products for orbit computations. The total ERP can be described as

$$\vec{f}_{ERP} = \sum_{j=1}^{N} \sum_{i=1}^{n} \frac{1}{m} \left(\vec{C}_{R,i} f_s P_{REF}^{j} + \vec{C}_{E,i} P_{EMT}^{j} \right) \tag{7}$$

where j is the index of a grid with N bins, $N = 72 \times 144$ for a resolution of $2.5^\circ \times 2.5^\circ$. The computations of P_{REF} and P_{EMT} need to modify a few aspects based on Eq. 5: firstly, all radiations originate from the top of the Earth's atmosphere (ToA, 30 km), rather than from the Sun. Secondly, P_{REF} depends on the illumination status of the Earth, whereas P_{EMT} does not. Thirdly, for the computation of $\vec{C}_{R,i}$, Eq. 6 can be used when the Sun-satellite vector is replaced by the ToA element-satellite vector. In addition, the computation of $\vec{C}_{E,i}$ has to specifically use the material characteristics (again absorption, specular reflection and diffuse reflection) for the long-wavelength infrared radiation. Fig. 4 shows that ERP has the largest component in radial direction. The scale factors for ERP are not estimated (fixed to 1) otherwise potential erroneous PCO or CoM offsets will turn into radial orbit shifts, which might be problematic for particularly altimetry missions e.g. Sentinel-3.

3.3. Aerodynamic Force

The thermosphere consists of neutral atoms and charged particles that are interacting with the satellite surfaces. Two component forces can be distinguished by definition, drag is the projection of AF onto the velocity direction with respect to the atmosphere and lift is the portion of AF perpendicular to the velocity direction. Nevertheless lift normally only accounts for a small proportion, e.g. for the Swarm-C satellite it is at a level of 1 nm/s^2, comparing to its drag at a level of 50 nm/s^2. AF is heavily dependent on the orbit altitude and the dominating force for LEO satellites flying at very low altitude, e.g.

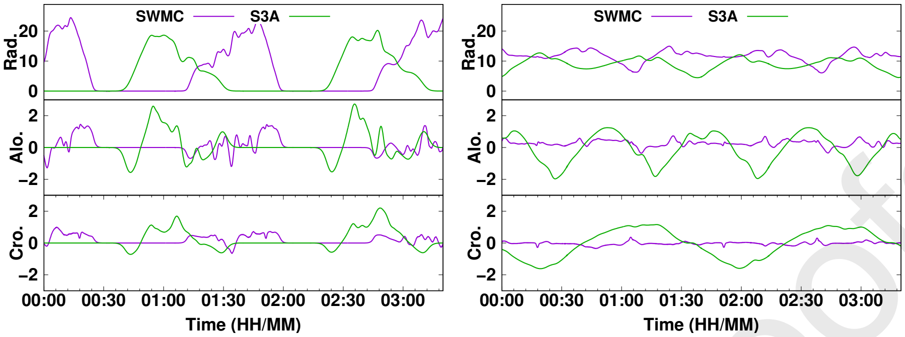

Figure 4: Earth reflectivity (left) and emissivity (right) radiation pressure for the Swarm-C and Sentinel-3A satellites (no scale factors applied). Please note that different axis limits are applied. Selected period: 7 June, 2018 (DOY:158) 00:00-03:20. Unit: $[nm/s^2]$.

the CHAMP, GOCE, GRACE and Swarm satellites (Visser et al., 2009; Mao, 2019a). AF can be described as

$$\vec{f}_{AF} = -\frac{\rho}{2m}\sum_{i=1}^{n} A_i \vec{v_i}^2 (C_{D_i}\vec{e}_{D_i} + C_{L_i}\vec{e}_{L_i}) \tag{8}$$

where $C_{D,L}$ denotes the coefficients for drag and lift, which can be modeled by algorithms such as Goodman, Sentman and SESAM (Doornbos, 2012; Girardin, 2016; Pilinski et al., 2013); $\vec{v_i}$ represents the relative velocity between a satellite plate and the atmosphere. The upper thermosphere can be very dynamic such that the Horizontal Wind Models (HWM), which reflect the time-varying atmospheric circulation dynamics, are needed to compute a most realistic relative velocity (Drob et al., 2015). As for the Swarm-C satellite, this contributes roughly a few nm/s^2 to AF particularly in cross-track direction for polar orbits.

A precise modeling of AF necessitates high-precision atmospheric models. Fig.5 compares the variations of two popular atmospheric models, ~~NRLMSISE2000 (Picone et al., 2002) and DTM2013~~ NRLMSISE-2000 (Picone et al., 2002) and DTM-2013 (Bruinsma, 2015), as modeled on the Sentinel-3A and Swarm-C satellites. The Sentinel-3A satellite orbits at an altitude of about 800 km, where the density is smaller by a factor of 100 than that for the Swarm-C satellite (500 km). The difference between the two atmo-

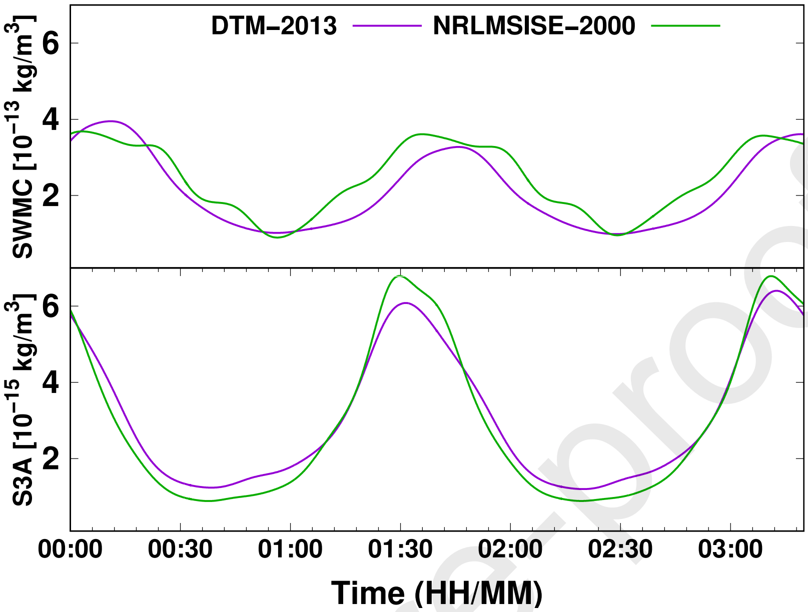

Figure 5: Atmospheric density models ~~DTM2013~~ DTM-2013 and ~~NRLMSISE2000~~ NRLMSISE-2000 density comparison for the Swarm-C (top) and Sentinel-3A (bottom) satellites ~~, note~~ in the ~~numbers are intentionally scaled to fit into the same axis limits (no~~ unit of kg/m^3. No scale factors are applied~~)~~. Selected period: 7 June, 2018 (DOY:158) 00:00-03:20.

spheric density models is less than 10% during the selected period (Bruinsma, 2015), and no significant impacts on the POD performances are witnessed in BSW when estimating scale factors and PCAs.

4. Results and Discussion

This section first includes a quality assessment of the associated GPS data, followed by internal consistency checks and external validations to different orbit solutions.

4.1. Data Quality Assessment

As outlined in Sect.1, 573 days are analyzed in this article. The selected period includes the so-called *tandem phase* (from 7 June, 2018 to 14 October, 2018) for the Sentinel-3A and -3B satellites, which were maintained at a separation of about 30 s to calibrate and validate the instrument packages onboard the Sentinel-3B satellite (Molina et al., 2019). Many days close to this phase are excluded from analysis due to large satellite maneuvers and data gaps. These account for 23 days for the Sentinel-3A satellite and 30 days for the Sentinel-3B satellite, respectively. Two additional days are excluded for the Sentinel-3B satellite due to problematic IAR. Besides that, 3 days are excluded for the Swarm-C satellite. The three satellites are equipped with similar 8-channel dual-frequency high-precision GPS receivers provided by *RUAG space* (Montenbruck et al., 2018a,b). The one integrated on the Sentinel-3B satellite has a new capability of tracking the GPS L2C signal with a similar overall performance (Molina et al., 2019), however in this article these observations are not used. The application of our internally generated PCV maps using the ~~*Residual Approach*~~*residual approach*, as well as the recommended Sentinel-3 GPS antenna PCO values and CoM corrections, is essential to fully exploit the precision of in-flight GPS observations for POD (Jäggi et al., 2009; Peter et al., 2017; Montenbruck et al., 2018a).

~~Tab.?? displays the performances of the *KNFA* POD solution for the three GPS receivers. As stated in Sect.2, a kinematic solution best reflects the quality of GPS observations.~~ The data editing process (mostly 4 cm to ~~phase~~carrier-phase, as introduced in Tab.2) only screens out about 3.4% observations, i.e. all integrated *RUAG Space* GPS receivers perform exceptionally good. The same batch of screened GPS observations are used for generating all the associated orbit solutions. The Swarm-C GPS receiver tracks slightly more GPS satellites (on average 7.55 for the Swarm-C satellite per epoch, 7.42 for the Sentinel-3 satellites) due to its lower orbit and hence better high-low geometry between a GPS receiver and the GPS constellation. Besides that, during the selected period the Swarm-C GPS receiver antenna field of view was 88°, larger than the 83° of the Sentinel-3 satellites (Van den IJssel et al., 2016; Molina et al., 2019). Eventually only less than 0.4% epochs miss valid kinematic orbit solutions for the Swarm-C satellite, and less than 0.1% for the two Sentinel-3 satellites. ~~The~~

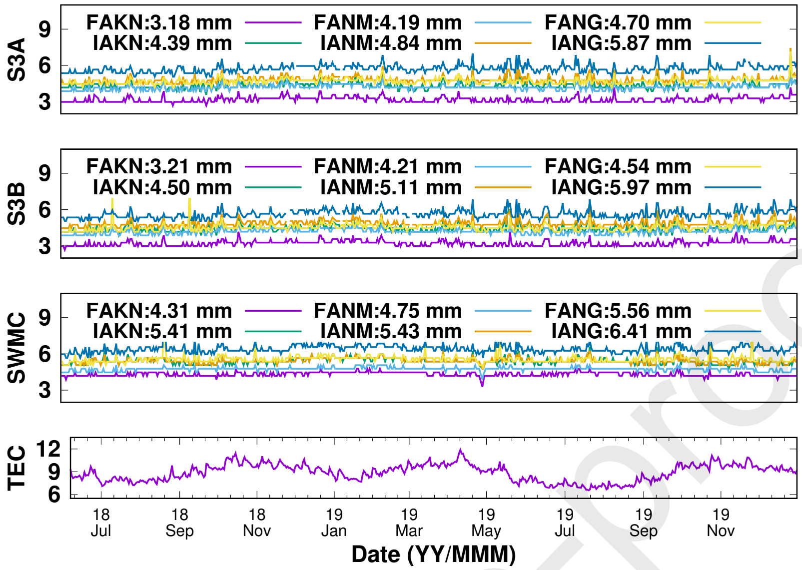

Figure 6: Daily ionosphere-free carrier-phase residuals for the different satellite orbit solutions and the total electron content. Selected period: 7 June, 2018 to 31 December, 2019. Residual unit: [mm], TEC unit: [TECU]

Fig.6 displays the ionosphere-free ~~phase~~ carrier-phase residuals of the different POD solutions for the three GPS receivers. As stated in Sect.2, a kinematic solution best reflects the quality of GPS observations. The *FAKN* carrier-phase residuals of the two Sentinel-3 GPS receivers are at a very good level of 3.2 mm. They perform better than the 4.3 mm of the Swarm-C GPS receiver, which experiences more signal disturbances due a lower orbit and a larger antenna field of view, which leads to noisier observations at especially the low elevations (Van den IJssel et al., 2016). In fact, the Swarm GPS receiver's performances are heavily dependent on ionospheric activities, and more extendedly, on solar activity cycles (Schreiter et al., 2019). In the past a few modifications were applied to the Swarm GPS receivers, leading to significantly improved absolute and relative POD services which also strengthened the associated Earth's gravity field recovery from kinematic positions ~~(Van den IJssel et al., 2016; Dahle et al., 2017; Mao et al., 2018; ?)~~

(Dahle et al., 2017; Mao et al., 2018; Teixeira da Encarnação et al., 2020). Besides that, it has to be noted that the selected period is in a solar minimum season and the last peak occurred around 2014. When referring to the mean Total Electron Content Unit (TECU) published by CODE (Dach et al., 2015), it is only 8.9 TECU for the selected period in this article (June 2018 to December 2019), comparing with 29.2 TECU for the entire year of 2014.

Fig.6 shows that the inclusion of more satellite dynamics and in particular IAR lead to increased carrier-phase residuals. The number of estimation parameters and associated degrees of freedom has a significant impact on the levels of carrier-phase residuals. The kinematic solution, which estimates epoch-wise three-dimensional coordinates for the entire orbit arc, has the largest number of parameters and therefore shows the lowest level of carrier-phase residuals. When compared with a classical NM POD parameterization, the NG POD mitigates the estimation of constant accelerations and more tightly constrains the estimation of PCAs towards zero (Tab.1), leading to slightly higher level of carrier-phase residuals. Besides that, an IAR process significantly reduces the number of estimated float ambiguities and therefore smaller degrees of freedom, resulting into higher level of carrier-phase residuals. These agree well with conclusions made in (Montenbruck et al., 2009; Hackel, 2019).

~~S3B FAKN 3.20 7.42 96.58 99.99 S3B FANM 4.21 7.42 96.58 100.00 S3B FANG 4.54 7.42 96.58 100.00 S3B IAKN 4.50 7.42 96.58 99.99 S3B IANM 5.11 7.42 96.58 100.00 S3B IANG 5.97 7.42 96.58 100.00 0.1em~~

~~SWMC FAKN 4.32 7.55 96.55 99.69 SWMC FANM 4.75 7.55 96.55 100.00 SWMC FANG 5.56 7.55 96.55 100.00 SWMC IAKN 5.41 7.55 96.55 99.69 SWMC IANM 5.43 7.55 96.55 100.00 SWMC IANG 6.41 7.55 96.55 100.00~~

The follow-up single-receiver IAR also ~~benefit~~ benefits from high-quality GPS observations. During the selected period there are around 410 integer ambiguities per day when processing observations from the two Sentinel-3 GPS receivers, and around ~~423~~ 420 for the Swarm-C GPS receiver. These are in good accordance with the mean of the used GPS satellites~~as listed in Tab. ??.The~~

~~Statistics of the ionosphere-free phase residuals, the mean of tracked GPS satellites (occupied tracking channels) after data screening, the percentage of used GPS observations and the percentages of epochs with valid kinematic solutions for the three GPS receivers.Note thatonly the *KNFA* orbit solutions are analyzed.~~

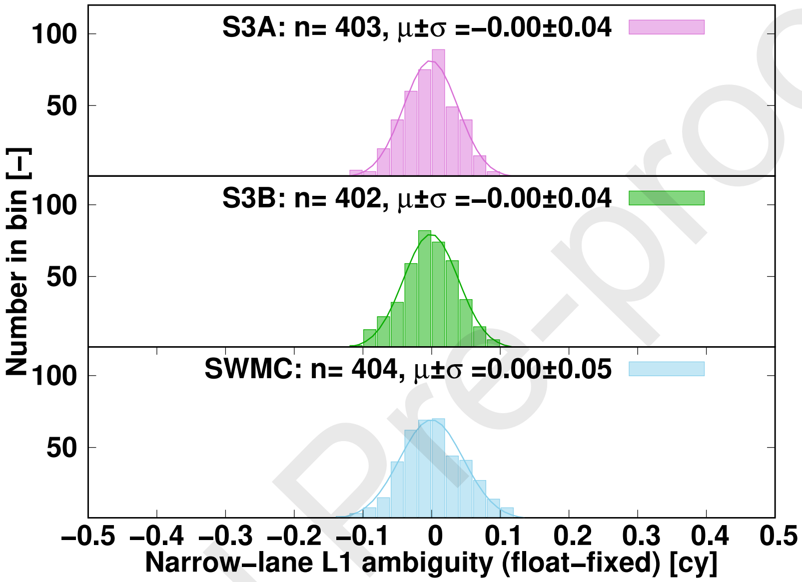

~~Satellite Solution Res. mmNo.Sats.-Data%Perc %S3A FAKN 3.17 7.42 96.58 99.97 S3A FANM 4.19 7.42 96.58 100.00 S3A FANG 4.70 7.42 96.58 100.00 S3A IAKN 4.39 7.42 96.58 99.97 S3A IANM 4.84 7.42 96.58 100.00 S3A IANG 5.87 7.42 96.58 100.00 0.1cm~~

Figure 7: Distribution of relative narrow-lane N_1 ($L1$) ambiguity fractional cycles of the three GPS receivers on 7 June, 2018 (DOY: 158). Gaussian distribution with the corresponding standard deviation is shown by each curve.

~~final~~. Fig.7 indicates that for the example day (7 June, 2018), 99.7% (3σ) of the Sentinel-3 narrow-lane ambiguity ~~resolution success rates~~ residuals are less than merely 0.12 cycles by magnitude, and slightly larger of 0.15 cycles for the Swarm-C GPS receiver, all foreseeing high success rates of integer rounding for the narrow-lane IAR. The analysis for the Sentinel-3A GPS receiver is slightly better than the research done in (Montenbruck et al., 2018b), which analyzed an earlier example day (4 April, 2016). Eventually, the narrow-lane IAR success rates for the Sentinel-3A, -3B and Swarm-C GPS receivers are 99.9%, 99.9% and 99.7% w.r.t. the fixed wile-lane integer ambiguities, and 99.0%, 99.2% and 95.9% w.r.t. all possible ambiguities, respectively. The IAR success rate for the ~~two Sentinel-3 GPS receivers are around 98%, slightly higher than the 95% for the~~ Swarm-C GPS receiver ~~experiencing~~ is slighty lower since it experiences more ionospheric disturbances ~~. A high success rate will guarantee~~ at a lower orbit and a larger antenna field of view. These high success rates will guarantee reliable and high-performance single-receiver IAR ~~POD~~orbit solutions in this article.

4.2. Internal Consistency Check

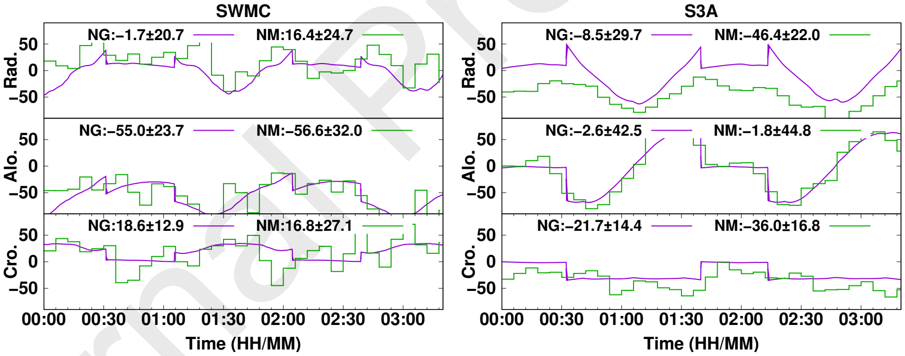

Figure 8: Comparison between the sum of all modeled non-gravitational forces (SRP and AF are scaled) from the *FANG* solution and the empirical acceleration estimated in the *FANM* solution. Left: the Sentinel-3A satellite (similar trend for the Sentinel-3B satellite.); Right: the Swarm-C satellite. Selected period: 7 June, 2018 (DOY:158) 00:00-03:20. Unit: $[nm/s^2]$.

For the *NM* orbit solution three constant empirical accelerations per orbit arc (24 h) and loosely constrained PCAs are estimated to compensate for the not explicitly modeled non-gravitational accelerations. In general, the three satellites need different levels of empirical accelerations. For along-track direction, where the aerodynamic drag dominates, the required empirical accelerations are consistent with the levels of aerodynamic drags. Fig.8 zooms into a short period, showing that the non-gravitational force modeling (NG) causes discrepancies of about $+37.9$ nm/s^2 and -18.1 nm/s^2 w.r.t the mean of the radial empirical accelerations co-estimated in the nominal orbit (NM) solutions for the Sentinel-3A and Swarm-C satellites, respectively. Tab.3 draws an overall statistics of the estimated empirical accelerations for the selected period. It is interesting to see that for the two identical Sentinel-3 satellites, there are differences of 12.4 nm/s^2 in radial direction and 1.7 nm/s^2 in cross-track direction for the co-estimated empirical accelerations of the $FANM$ orbit solutions. The consistency of the $FANG$ orbit solutions becomes significantly better. However, for the $IANG$ orbit solutions, a similar cross-track discrepancy of 1.5 nm/s^2 exist for the two Sentinel-3 satellite. These probably suggest remaining systematic differences in geometry offsets, e.g. in PCO or ARP, which is in line with Montenbruck et al. (2018a); Peter et al. (2020), who investigated the sensitivity of offsets estimation to the POD of the Sentinel-3A and Sentinel-1 satellites, respectively.

Table 3: Statistics of total empirical accelerations (as for NM solution, the sum of once-per-arc empirical acceleration and PCAs) estimate for three satellites, unit: [nm/s^2].

Sat.	Solution	~~Radial~~ Rad.	~~Along-track~~ Alo.	~~Cross-track~~ Cro.
S3A	FANM	-38.6 ± 24.1	-1.4 ± 46.3	-31.0 ± 20.6
S3B	FANM	-26.2 ± 23.9	-1.5 ± 46.0	-29.3 ± 20.8
SWMC	FANM	25.5 ± 29.1	-35.3 ± 34.9	4.4 ± 48.8
S3A	FANG	-0.5 ± 0.8	-0.1 ± 1.6	-0.1 ± 4.3
S3B	FANG	-0.3 ± 0.8	-0.1 ± 1.6	-0.0 ± 4.3
SWMC	FANG	1.3 ± 2.3	-0.0 ± 5.9	-0.0 ± 9.1
S3A	IANG	-0.7 ± 1.3	-0.1 ± 2.6	-0.5 ± 6.4
S3B	IANG	-0.4 ± 2.0	-0.1 ± 4.8	1.0 ± 6.4
SWMC	IANG	0.8 ± 3.5	0.1 ± 6.9	1.2 ± 12.0

The implementation of non-gravitational force modeling in the $FANG$ solution significantly reduces the required empirical accelerations that are used to mitigate satellite dynamic modeling deficiencies. Meanwhile, it has to be noted that the float ambiguities might be absorbing some systematic offsets, whereas the additional single-receiver IAR ($IANG$) solution is governed by slight larger PCAs (indicated by the larger STD statistics), although they are based on the same a-priori STD to constrain the PCAs. Besides, a mean offset of only $-0.5\ nm/s^2$ in cross-track direction appears in the $IANG$ solution of the Sentinel-3A satellite. Montenbruck et al. (2018a) reported a mean offset of around 9 nm/s^2 in the same direction, though for a period of 20 days in the earlier 2016. Montenbruck et al. (2018a) recommended a 1 cm correction to the CoM in the +Y direction (satellite body reference frame, approximately aligned with cross-track direction). This article uses the official CoM table with the proposed +1 cm correction for generating vectors pointing from CoM to ARP and LRR. The results confirm the value of the correction to CoM (Montenbruck et al., 2018a). Lastly, there might still exist constant but much smaller geometry offsets in cross-track direction for the three satellites, which may be addressed in future investigations.

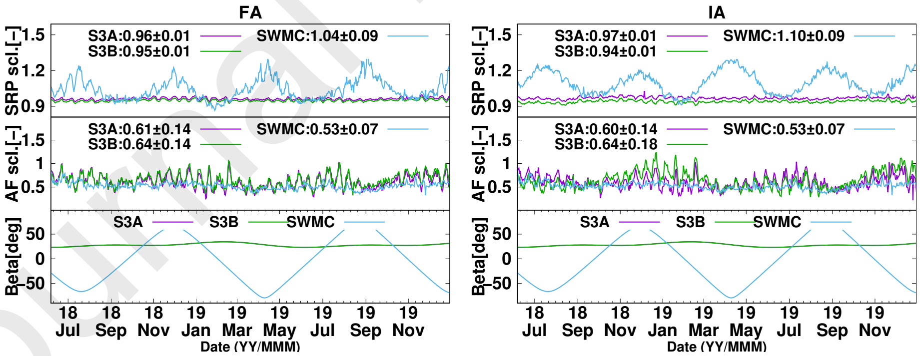

Figure 9: SRP and AF scale factor estimates for the three satellites without (FA, left) and with (IA, right) ambiguity resolution. Selected period: 7 June, 2018 to 31 December, 2019.

Fig.9 depicts the scale factor estimates for the non-gravitational forces. Note that the scale factors of AF for three satellites are generally smaller than 1, indicating an overestimated modeling performance. The AF modeling for the Sentinel-3 satellites might be very challenging since this satellite formation is placed into a much higher orbit where most of atmospheric density models are not accurate enough and often overestimate reality, particularly for low solar activity seasons (Bruinsma, 2015; He et al., 2018). Interestingly, it seems that the AF modeling for the Swarm-C satellite is also overestimated. Van den IJssel et al. (2020) investigated the POD performance for the Swarm-C satellite during an earlier period of approximately 9 months in 2017–2018 using the ~~GHOST software package~~ GPS High Precision Orbit Determination Software Tools (GHOST) (Wermuth et al., 2010), the mean of AF scale factors was 0.538 (please note the authors used a different atmospheric density model, ~~NRLMSISE2000~~NRLMSISE-2000). Our analysis for the Swarm-C data in 2018 provides a mean scale factor of 0.54, suggesting an approximate consistency between the AF modelings in the two POD software packages. In addition, the ~~DTM2013~~ DTM-2013 density model used in this article is ~~derived~~ based on the data from 1969 to 2012 (Bruinsma, 2015), and the current solar cycle (24th) has been experiencing significantly lower solar activities when compared with the past few cycles (Pesnell, 2016). That suggests a possible over-performing of this density model for the current solar minimum period. Another preliminary POD test is done to the Swarm-C satellite for March 2014, when solar activities were much stronger. As discussed in Sect.4.1, the TEC at that time was 2 times larger than during the selected period in this article. Indeed, the new estimate of the scale factor increases to 0.84, suggesting more precise modeling of AF during March 2014. Thanks to the significance of using scale factors, in general our POD strategies, as well as the similar approaches of the other investigations (Montenbruck et al., 2018a; Hackel, 2019; Van den IJssel et al., 2020; Peter et al., 2020; Vielberg and Kusche, 2020), are robust and flexible for different situations.

The estimated SRP scale factors are much closer to 1.0 - i.e. 0.96/0.97, 0.95/0.94 and 1.04/1.10 for the *FA*/*IA* POD solutions of the Sentinel-3A, -3B and Swarm-C satellites respectively - indicating a more realistic modeling of

SRPs. The SRP scale factor for particularly the Swarm-C satellite displays a strong correlation with the beta angle. It is, in particular, close to 1 when the beta angles are almost 0°. This result again agrees well with Van den IJssel et al. (2020) who obtained a mean scale factor of 1.077 for Swarm-C during a period of approximately 9 months in 2017–2018. In addition, Fig.9 shows that single-receiver IAR will slightly increase the differences between the mean of AF scale factors for the two Sentinel-3 satellites, with an slight increase of variability from 0.14 to 0.18 for the Sentinel-3B satellite. These suggest small orbit shifts caused by the extra constrains from IAR, which influence the estimate of the other parameters such as empirical accelerations and scale factors (Tab.3).

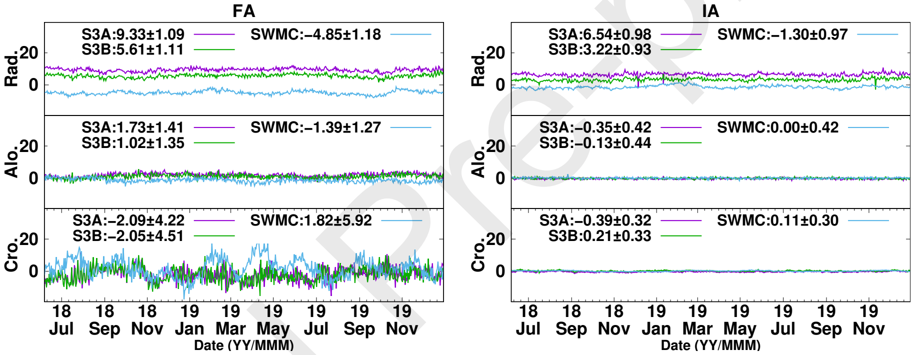

Figure 10: ~~Orbit~~ The daily mean of orbit comparisons between the non-gravitational force modeling (*NG*) reduced-dynamic orbit and its corresponding kinematic (*KN*) orbit for the three satellites without (*FA*, left) and with (*IA*, right) ambiguity resolution. Selected period: 7 June, 2018 to 31 December, 2019. Unit: [mm].

Fig.10 displays the comparison between the *NG* orbits and the corresponding *KN* orbits using the same set of either float or integer ambiguities. In general the three satellites all show a very good internal orbit consistency at a level of sub cm in the vertical (radial) direction, which is the largest component of Geometry Dilution Of Position (GDOP), and smaller in the horizontal (along-track and cross-track) directions (Mao, 2019a). The non-gravitational force modeling strategy clearly shifts satellite orbits in radial direction, i.e. for the

FA solutions 9.33, 5.61 and -4.85 mm for the Sentinel-3A, -3B and Swarm-C satellites, respectively. The different levels of shifts to the two identical Sentinel-3 satellites and the different sign to the Swarm-C satellite again suggest different potential offsets in the PCO information, particular in the *Up* direction in the satellite body-fixed reference frame (Peter et al., 2020). In addition, IAR further constrains the orbit in particular cross-track direction, where the STDs are reduced by a factor of more than 10, agreeing well with the conclusion made in (Montenbruck et al., 2018a). In this article, the cross-track orbit consistency between the *IANG* and *IAKN* solutions is only -0.39 mm for the Sentinel-3A satellite, which benefits significantly from the applied offset correction (+Y) to CoM. In addition, PCV maps might also induce cross-track offsets (Jäggi et al., 2009) depending on the approaches of being created, e.g. in this article PCV maps are created based on a reduced-dynamic POD using float ambiguities. The same PCV map is used for generating all orbit solutions for a satellite. This article does not correct possible remaining offsets and create PCV maps based on a reduced-dynamic POD using integer ambiguities.

4.3. External Orbit Validation

The inter-agency cross-comparison is crucial to monitor accuracy of the different BSW orbit solutions. An orbit validation is first carried out by comparing our orbit solutions with external orbit solutions generated using other independent POD software packages. Under the scheme of CPOD Service for the Sentinel satellites, the NAPEOS (Navigation Package for Earth Orbiting Satellites) software, which is the leading ESA/ESOC software for POD, has been used for providing the official orbit products for the Sentinel-3 satellites (Fernández et al., 2016). Besides that, the GHOST software, an eminent LEO POD software package developed by The German Space Operation Center (GSOC) with support from TU Delft, has been used for generating the Swarm Precise Science Orbits (PSO) products (Wermuth et al., 2010; Van den IJssel et al., 2015). Note that both software packages are able to generate various orbit solutions, e.g. kinematic and reduced-dynamic orbits, however herein only the reduced-dynamic orbit solutions including non-gravitational force modeling are used for comparisons.

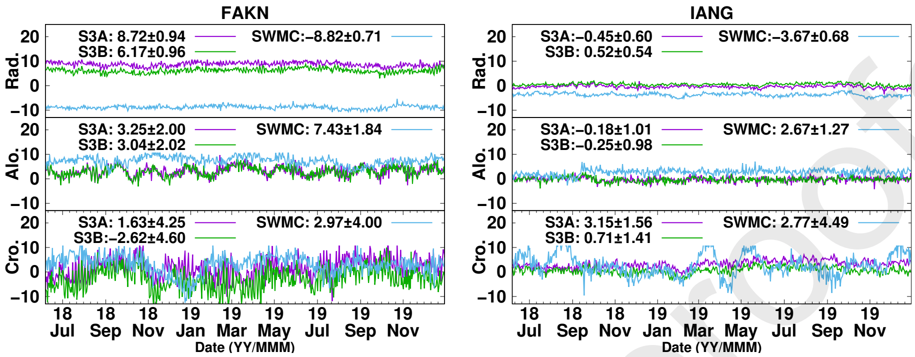

Figure 11: The daily mean of orbit comparisons between the *FAKN* (left) and *IANG* (right) orbit solutions from this article, and the independent Sentinel-3 CPOD orbits and Swarm-C PSO orbits. An outlier screening of 200 mm is applied. Selected period: 7 June, 2018 to 31 December, 2019. Unit: [mm].

Fig. 11 depicts the daily mean of orbit consistency between the BSW orbits and the external orbits for the full selected period. The consistency is displayed for the three directions referring to the local orbital reference frame. In general, both BSW orbits agree with the external orbits at a level of only sub cm. Comparisons with the same orbits clearly confirm the importance of non-gravitational force modeling, which shifts the orbits in radial direction by 9.17, 5.65 and -5.15 mm (i.e. *FAKN-IANG*) for the Sentinel-3A, -3B and Swarm-C satellites, respectively. Benefiting from the tighter constraints of IAR, the *IANG* orbit solution shows better agreement with the external orbits. The mean radial and along-track orbit agreements between the best BSW *IANG* Sentinel-3 orbits and the corresponding CPOD orbits are less than 1 mm. However, a discrepancy of 3.15 mm exists in cross-track direction for the Sentinel-3A satellite, suggesting a remaining cross-track CoM offset in one of the two comparing orbits. It is interesting to see that an radial discrepancy of -3.67 mm exists for the Swarm-C satellite when referring to the PSO orbit, again indicating potential PCO or ARP errors in the *Up* direction in the satellite body-fixed reference frame. AIUB and TUD both processed the associated Swarm-C GPS antenna PCV patterns internally and assumed an all-zero PCO for the Swarm satellites POD (Van den IJssel et al., 2015), where PCV patterns can also induce potential cross-track offsets that are visible in Fig. 11.

4.4. ~~External Orbit Validation~~

The International Laser Ranging Service (ILRS) allows an independent validation of the GPS-based orbit solutions in the line-of-sight directions between the SLR ground stations and the three satellites (Pearlman et al., 2002). Ten SLR stations (Yarragadee, ~~Greenbelt, Haleakala, Hartebeesthoek, Zimmerwald, Graz, Herstmonceux, Potsdam, Matera, Wettzell) with~~ Australia; Greenbelt, USA; Haleakala, Hawaii-USA; Hartebeesthoek, South Africa; Zimmerwald, Switzerland; Graz, Austria; Herstmonceux, UK; Potsdam, Germany; Matera, Italy; Wettzell, Germany) with good global observing geometry and high performance are used for the orbit evaluation. To eliminate spurious and bad observations, an editing threshold of ~~20 cm~~ 200 mm is used, which is more than an order of magnitude above the RMS of fit levels, and observations below a 10° elevation cutoff angle are excluded. The LRR correction patterns for the associated satellites have to be included (Arnold et al., 2019). Exactly the same SLR validation scheme is used for all types of orbit solutions. Ultimately, 83.4%, 86.4% and 86.4% of all the available SLR measurements are used for the Sentinel-3A, Sentinel-3B and Swarm-C satellites, respectively. On average roughly 50 normal points are available for the Swarm-C satellite orbit validation per day, reasoning that the Swarm-C satellite has been maintained in a close pendulum formation with the Swarm-A satellite that occupies some tracking opportunities (Mao et al., 2019b). The number of normal points for both Sentinel-3 satellites is ~~larger than~~ roughly 100 due to their higher orbit, and more importantly, due to their ~~180° orbit separation (except for~~ 140° orbit phase separation excluding the short *tandem phase* ~~)~~(Fernández et al., 2016).

Tab.4 shows the agreements between the different orbit solutions and inde-

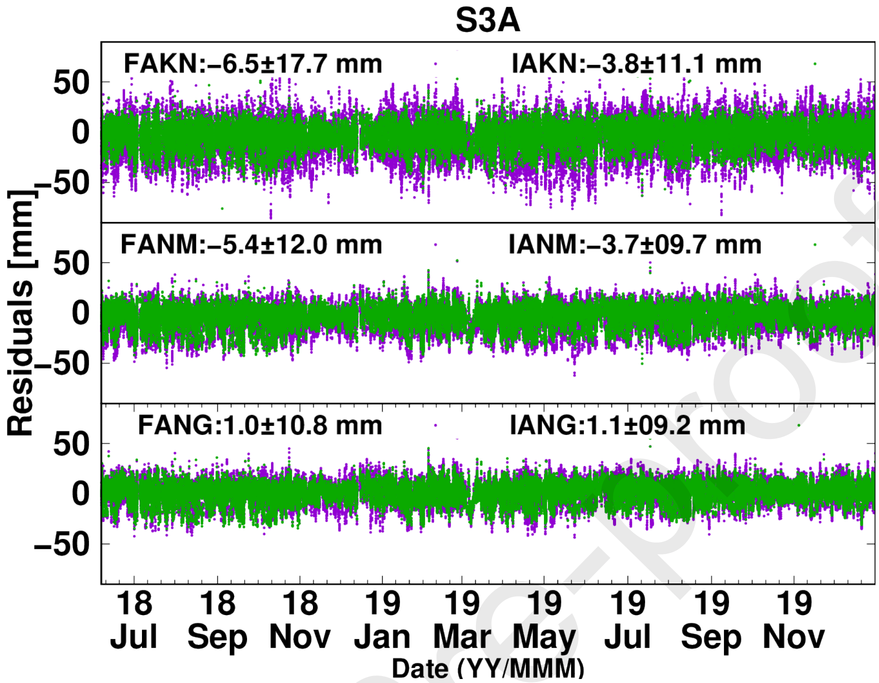

Figure 12: Satellite laser ranging validations for the different orbit solutions of the Sentinel-3A satellite. Selected period: 7 June, 2018 to 31 December, 2019.

pendent SLR measurements. Residuals can be used to estimate orbit offsets in each component direction of the local orbital reference frame based on the method described in (Arnold et al., 2019). The SLR validation statistics confirm that all types of orbit solutions generated using BSW, as well as the Sentinel-3 CPOD orbits and the Swarm-C PSO orbit, show orbit precisions of smaller than 20 mm. Although the BSW kinematic orbits show the largest STD, which is normal for a pure kinematic LEO POD strategy, these orbit precisions still meet the proposed requirements (Fernández et al., 2016). In fact the kinematic orbit solutions based on fixed ambiguities are only marginally ~~above~~ inferior to the reduced-dynamic and dynamic orbit solutions, showing the limitations of SLR to distinguish between the different orbit types.

The *KN* and *NM* orbit solutions heavily rely on the correctness of all offsets and CoM coordinates (Jäggi et al., 2009), whereas the *IANG* orbit solutions are largely independent of wrong GPS antenna offset or CoM coordinates and are thus mainly validating the modeled dynamics. In this article, the slightly different radial offsets of *KN* orbit solutions (preferably ambiguity-fixed *IAKN* orbit solutions) indicate a small inconsistency in the ARPs for the Sentinel-3A and -3B twin satellites. These can be also confirmed by comparing with the CPOD orbits, which are computed with a refined profile of satellite non-gravitational force modeling (Peter et al., 2017; Fernández et al., 2019). The very small offsets of the *IANG* orbit solutions indicate that the dynamics is well modeled for the two Sentinel-3 satellites, significantly reducing the mean offsets in particular radial and cross-track directions from a few mm to a remaining level of 1 mm. The two Sentinel-3 satellites were launched with a separation of more than 2 years, their macro-models might experience different material aging throughout the mission period. In addition, there are still about ~~2~~2.7 mm remaining offsets for the Swarm-C satellite, whereas the PSO orbits show an offset of only 0.6 mm. The dynamic modeling for the Swarm-C satellite seems to indicate a ~~discrepancy~~slight discrepancy when compared with the PSO orbits, similar as reflected in the SRP scale factors of larger than 1 (Fig.9) ~~.~~ and the remaining 2-3 mm orbit offsets in the direct inter-agency orbit comparisons (Fig. 11). This also suggests possible errors in ~~its~~ the Swarm-C macro-model, and in fact, ESA has been occasionally updating the Swarm thermo-optical properties during the past years (Siemes, 2020). The macro-models introduced in ~~(Montenbruck et al., 2018b; Fernández, 2019a)~~ (Montenbruck et al., 2018b) might need to be modified.

Fig.12 shows the SLR validation residuals of the different orbit solutions for the example Sentinel-3A satellite. Fig.13 depicts the nadir- and azimuth-dependent distribution of the associated residuals for the same satellite. They show the gradual improvement of orbit solutions by including more benefits from IAR and non-gravitational force models. A significant reduction of the mean of all residuals is obtained when comparing between the *FAKN* and *IANG* orbit solutions. There seem to be a slightly larger systematic residual pattern existing in cross-track direction, however this can be reduced to a much lower level by IAR and the *IANG* orbit solution shows the best agreement with SLR measurements. Eventually, after applying the two LEO POD advances in BSW, better orbits can be achieved and the final precisions are at levels of close to merely 9 mm for the three satellites. These precisions are even slightly better than the currently operational CPOD and PSO orbits. However, it has to be noted that both the NAPEOS and GHOST software packages that are used to generate these external orbits, also have the capability of single-receiver IAR that leads to better orbit solutions (Montenbruck et al., 2018b; Peter et al., 2020; Van den IJssel et al., 2020).

Table 4: Mean and STD statistics of SLR residuals in the line-of-sight direction and mean offsets in the local orbital reference frame for the three satellites using normal points collected by 10 selected stations. Note that the estimated orbit offsets are not applied, as can be done in (Arnold et al., 2019). (Elevation cut-off angle: 10 deg, outlier screening: 200 mm, selected period: 7 June, 2018 to 31 December, 2019. unit: [mm].~~The smallest number for the *FA*~~) ~~solutions are marked in green, those for the *IA*solutions are marked in blue).~~

Satellite	Solutions	Mean	STD	Rad.	Alo.	Cro.
S3A	FAKN	-6.5	17.7	-9.8	-3.1	2.4
S3A	FANM	-5.4	12.0	-7.6	-4.2	4.8
S3A	FANG	1.0	10.8	1.8	-1.5	-0.6
S3A	IAKN	-3.8	11.1	-6.0	0.2	2.2
S3A	IANM	-3.7	9.7	-5.8	0.2	1.5
S3A	IANG	1.1	9.2	1.6	-0.2	1.1
S3A	CPOD	1.4	12.7	1.9	1.7	4.8
S3B	FAKN	-5.1	18.5	-7.8	0.3	6.2
S3B	FANM	-3.8	12.4	-5.5	-0.6	7.7
S3B	FANG	0.1	10.8	0.5	1.0	3.3
S3B	IAKN	-2.3	11.1	-3.8	2.9	3.6
S3B	IANM	-2.3	9.6	-3.8	2.9	3.0
S3B	IANG	0.3	9.2	0.3	2.7	3.0
~~0.2cm~~S3B	CPOD	0.6	12.6	0.5	4.7	3.0
SWMC	FAKN	~~4.5~~ 4.9	15.7	~~7.8~~ 8.4	~~-2.3~~-1.4	~~-2.1~~-2.2
SWMC	FANM	~~4.8~~ 5.1	~~11.6~~ 11.4	~~8.5~~ 9.0	~~-3.6~~ -3.1	~~-3.2~~ -3.1
SWMC	FANG	~~1.9~~2.1	11.6	~~4.0~~4.5	~~-6.9~~ -6.7	~~-3.0~~ -2.9
SWMC	IAKN	~~2.1~~2.3	~~10.2~~ 10.1	~~3.0~~3.5	~~1.5~~ 1.4	~~-3.4~~ -3.3
SWMC	IANM	~~2.7~~ 3.0	~~9.0~~ 8.9	~~4.0~~ 4.5	~~1.5~~ 1.3	~~-3.1~~-3.0
SWMC	IANG	~~2.5~~ 2.7	~~9.0~~8.8	~~3.7~~ 4.1	~~1.4~~1.2	-3.2
SWMC	PSO	0.6	12.7	-0.2	4.3	-0.3

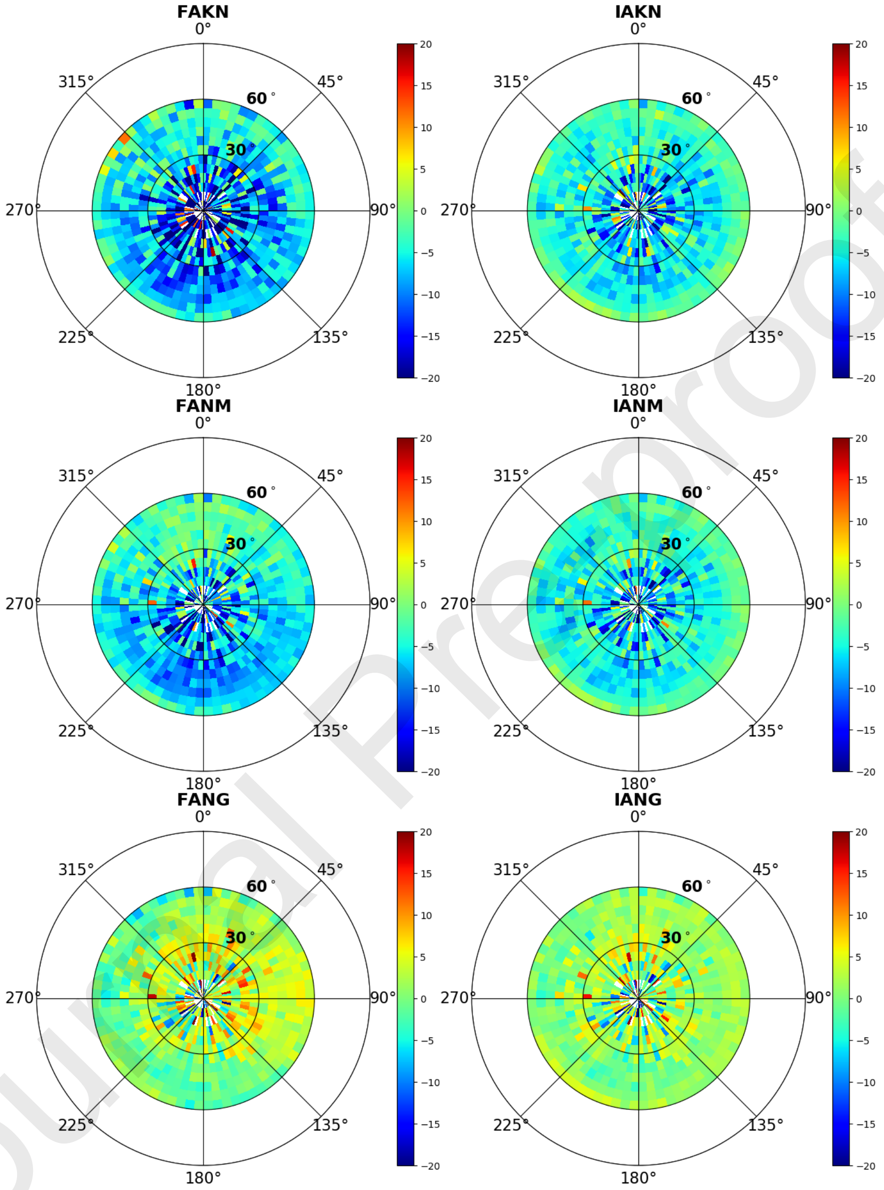

Figure 13: The Sentinel-3A SLR orbit validation residual distribution as a function of azimuth and nadir angle as seen in the LRR reference frame. An elevation cut-off angle of 10° as seen from SLR stations to the satellite result into nadir angles below 61.1°. Note that the +Y axis (Azimuth=0°) approximately aligns with cross-track direction. The binning resolution is 5° × 5° and each bin displays averaged value of at least 2 residuals. Selected period: 7 June, 2018 to 31 December, 2019. Unit: [mm].

5. Summary and Outlook

This article investigates the latest development of the Bernese GNSS Software for low Earth orbit satellite precise orbit determination. The focus of the new strategy is based on a refined dynamic modeling of satellites. Three main non-gravitational forces - solar radiation pressure, Earth radiation pressure and aerodynamic force - are modeled as the sum of independent plate-wise surface force acting on a satellite macro-model. The non-solar plates are assumed to spontaneously re-emit all absorbed energy after receiving radiation pressures from both the Sun and the Earth. The modeling of Earth radiation pressure further takes into account of the Earth's Radiant Energy System S4 grid products, and a set of monthly products are created by averaging data from the past 19 years. A linear interpolation has to be done between two neighboring months. Besides, the GNSS Observation-Specific Bias (OSB) and ambiguity fixed clock products provided by the Center for Orbit Determination in Europe (CODE) allow for single-receiver integer ambiguity resolution which further constrains the associated orbit solutions.

GPS data of three Earth observation satellites - Sentinel-3A, Sentinel-3B and Swarm-C - are processed for a time span of 1.5 years between June 2018 and December 2019. Firstly, the empirical accelerations, that are supposed to compensate for deficiencies in the satellite dynamic modeling, can be partially replaced by the non-gravitational force modeling. For instance, statistics of the mean of three dimensional (radial, along-track and cross-track referring to the local orbital reference frame) empirical accelerations for the Sentinel-3A satellite can be significantly reduced from $-38.6/-1.4/-31.0\ nm/s^2$ to below $1\ nm/s^2$ in the three directions. The standard-deviations are also reduced to much lower levels due to tighter constraints (by a factor of 10, Tab.1)~~and~~ , and more importantly, the non-gravitational force modeling. For the situations where the supporting models for non-gravitational forces can not fully represent the real in-flight environment, the co-estimated corresponding scale factors will adjust the associated forces, e.g. the over-performed aerodynamic forces modeling can be adjusted by scale factors smaller than 1. This is consistent with LEO POD performance using the GHOST software package (Van den IJssel et al., 2020). The modeling of solar radiation pressure has been very stable and no extra scale factors are estimated for the Earth radiation pressure to maintain its neutral contributions to shift orbits particularly in radial direction. In addition, the integer ambiguity fixing brings more tightly constrained geometry to the satellite positions.

Finally, the best possible orbits can be obtained by combining all these benefits. The satellite laser ranging validations show orbit precisions of 9.2, 9.2 and ~~9.0~~8.8 mm for the Sentinel-3A, Sentinel-3B and Swarm-C satellites, respectively. The different comparisons again prove a superior performance of the new POD strategy, however also indicate a few small issues to the accuracy of the coordinates of the satellite ~~Center of Mass (CoM)~~ center of mass and instrument reference points.

As a member of the Copernicus Precise Orbit Determination (CPOD) Quality Working Group (QWG) for the Sentinel satellites, the Astronomical Institute of the University of Bern (AIUB) has been routinely processing better orbits (in this article labeled as *IANG*) than the previous solutions (*FANM*) since these software modifications were made to BSW. The independent satellite laser ranging validation also confirms a slightly better orbit precision when compared with the CPOD orbit. Recent Sentinel Regular Service Review (RSR) reports have shown that the AIUB solutions currently agree best with the combined orbits for all contributing QWG solutions, and larger weights are thus applied to the AIUB orbit solutions when generating the final combined orbits ~~(Fernández, 2019c; ?)~~(Fernández, 2019b,c). More reports can be found via https://sentinel.esa.int/web/sentinel/~~missions~~technical-guides/~~sentinel-3~~sentinel-3-altimetry/~~ground-segment/~~ (~~accessed: 8 June~~Last accessed: 12 September, 2020).

Future work can be also put on investigating the more challenging estimate of the trajectory satellite ~~CoM~~ center of mass and the satellite macro-model, which might further reduce the uncertainties within the precise orbit determination process. In addition, ~~(Jäggi et al., 2009)~~ Jäggi et al. (2009) did a simulation study which showed that the Phase Center Variation (PCV) maps need to be simultaneously estimated with other orbit parameters. It might be an interesting topic to iterate new PCV maps based on the non-gravitational force modeling and integer ambiguity resolution.

Acknowledgment

This research was funded by the Swiss National Science Foundation (Grant 200021-169035) and the European Research Council under the grant agreement No. 817919 (project SPACE TIE). All views expressed are those of the authors and not of the agency. We would also like to show our special gratitude to the European Space Agency and the Copernicus Precise Orbit Determination service for kindly sharing the associated satellite data products. Calculations were performed on UBELIX (http://www.id.unibe.ch/hpc), the HPC cluster at the University of Bern. The generous support of the three anonymous reviewers is also gratefully acknowledged.

References

Arnold, D., Schaer, S., Villiger, A., et al., 2018. Undifference ambiguity resolution for GPS-based precise orbit determination of low Earth orbiters using the new CODE clock and phase bias products, in: International GNSS Service Workshop 2018, 29 Oct.-02 Nov. 2018, Wuhan, China.

Arnold, D., Montenbruck, O., Hackel, S., et al., 2019. Satellite laser ranging to low Earth orbiters: orbit and network validation. J. Geod. 93(11):2315–2334. doi:10.1007/s00190-018-1140-4.

Berger, M., Moreno, J., Johannessen, J.A., et al. ESA's Sentinel missions in support of Earth system science. Remote Sens. Environ. 120:84-90. doi:10.1016/j.rse.2011.07.023.

Bertiger, W., Desai, S.D., Haines, B., et al., 2010. Single receiver phase ambiguity resolution with GPS data. J. Geod. 84(5):327–337. doi:10.1007/s00190-010-0371-9.

Beutler, G., Bauersima, I., Gurtner, W., et al., 1987. Evaluation of the 1984 Alaska Global Positioning System campaign with the Bernese GPS software. J. Geophys. Res. Solid Earth 92(B2):1295–1303. doi: 10.1029/JB092iB02p01295.

Bezděk, A., and Sebera, J., 2013. Matlab script for 3D visualizing geodata on a rotating globe. Comput. Geoscis. 56:127–130. doi:10.1016/j.cageo.2013.03.007.

Bock, H., Jäggi, A., Meyer, U., et al., 2011. GPS-derived orbits for the GOCE satellite. J. Geod. 85(11):807-818. doi:10.1007/s00190-011-0484-9.

Bruinsma, S., 2015. The DTM-2013 thermosphere model. J. Space Weather. Space Clim. 5(A1):1-8. doi:10.1051/swsc/2015001.

Cerri, L., Berthias, J.P., Bertiger, W.I., et al., 2010. Precision orbit determination standards for the Jason series of altimeter missions. Mar. Geod. 33(S1):379–418. doi:10.1080/01490419.2010.488966.

Dach, R., Lutz, S., Walser, P., et al., 2015. Bernese GNSS software version 5.2. Technical Report. Astronomical Institute, University of Bern. doi:10.7892/boris.72297.

Dach, R., Schaer, S., Arnold, D., et al., 2019. Center for Orbit Determination in Europe (CODE): Technical Report 2018. IGS Central Bureau and University of Bern, Bern Open Publishing, pp 31-46, July 2019. doi:10.7892/boris.130408.

Dahle, C., Arnold, D., and Jäggi, A., 2017. Impact of tracking loop settings of the Swarm GPS receiver on gravity field recovery. Adv. Space Res. 59(12):2843–2854. doi:10.1016/j.asr.2017.03.003.

Dehant, V., Defraigne, P., Wahr, J.M., 1999. Tides for a convective Earth. J. Geophys. Res. Solid Earth 104(B1):1035–1058. doi:10.1029/1998JB90005.

Doornbos, E., 2012. Thermospheric density and wind determination from satellite dynamics. PhD thesis, Delft University of Technology, ISBN:978-3-642-44264-3.

Drob, D.P., Emmert, J.T., Meriwether, J.W., et al., 2015. An update to the Horizontal Wind Model (HWM): The quiet time thermosphere. Earth Space Sci. 2(7):301–319. doi:10.1002/2014EA000089.

Fernández, J., Escobar, D., Peter, H., et al., 2015. Copernicus POD service operations — orbital accuracy of Sentinel-1A and Sentinel-2A. In: Proc. Int. Symp. Space Flight Dynamics 2015, pp:1–14. 19 Oct.-23 Oct. 2015, Munich, Germany.

Fernández, J., Fernández, C., Féménias, P., et al., 2016. The Copernicus Sentinel-3 mission. In: The 20th International Laser Ranging Workshop 2016, pp: 1–4. 09 Oct.–14 Oct. 2016, Potsdam, Germany.

Fernández, J., Peter, H., Calero, E.J., et al., 2019. Sentinel-3A: validation of orbit products at the Copernicus POD service. In: Mertikas S., Pail R. (eds) Fiducial Reference Measurements for Altimetry. International Association of Geodesy Symposia, 150:75-82. Springer, Cham. doi:10.1007/1345_2019_64.

Fernández, M., 2019a. Sentinel-3A properties for GPS POD, GMV-GMESPOD-TN-0027, v1.7, 18/11/2019. Technical Report. GMV innovating solutions, url: https://sentinel.esa.int/documents/247904/3372613/Sentinel-3-GPS-POD-Properties.pdf (last accessed: 12 Sep., 2020).

Fernández, M, 2019b. Copernicus for Regular Service Review, Feb-May 2019: Copernicus Sentinel-1, -2 and -3 precise orbit determination service (SENTINELS POD), GMV-GMESPOD-RSR-0014, v1.1, 19/7/2019. Technical Report. GMV innovating solutions, url:

https://sentinel.esa.int/web/sentinel/technical-guides/sentinel-3-altimetry/pod/documentation (last accessed: 12 Sep., 2020).

Fernández, M., 2019c. Copernicus for regular service review, Jun-Sep 2019: Copernicus Sentinel-1, -2 and -3 precise orbit determination service (SENTINELS POD), GMV-GMESPOD-RSR-0015, v1.0, 31/10/2019. Technical Report. GMV innovating solutions, url: https://sentinel.esa.int/web/sentinel/technical-guides/sentinel-3-altimetry/pod/documentation (last accessed: 12 Sep., 2020).

Friis-Christensen, E., Lühr, H., Knudsen, D., et al., 2008. Swarm - an Earth observation mission investigating geospace. Adv. Space Res. 41(1):210–216. doi:10.1016/j.asr.2006.10.008.

Girardin, V., 2016. Impact of non-gravitational forces on GPS-based precise orbit determination of low Earth orbiters. Master thesis, Delft University of Technology.

Hackel, S., Montenbruck, O., Steigenberger, P., et al., 2017. Model improvements and validation of TerraSAR-X precise orbit determination. J. Geod. 91(5):547–562. doi:10.1007/s00190-016-0982-x.

Hackel, S., 2019. Refinement of reduced-dynamic orbit determination for low Earth satellites. PhD thesis, Technische Universität München.

He, C., Yang, Y., Carter, B., et al., 2018. Review and comparison of empirical thermospheric mass density models. Prog. Aerosp. Sci. 103: 31–51. doi:10.1016/j.paerosci.2018.10.003.

Jäggi, A., Hugentobler, U., and Beutler, G., 2006. Pseudo-stochastic orbit modeling techniques for low-Earth orbiters. J. Geod. 80(1):47–60. doi:10.1007/s00190-006-0029-9.

Jäggi, A., Hugentobler, U., Bock, H., et al., 2007. Precise orbit determination for GRACE using undifferenced or doubly differenced GPS data. Adv. Space Res. 39(10):1612-1619. doi:10.1016/j.asr.2007.03.012.

Jäggi, A., Dach, R., Montenbruck, O., et al., 2009. Phase center modeling for LEO GPS receiver antennas and its impact on precise orbit determination. J. Geod. 83(12):1145–1162. doi:10.1007/s00190-009-0333-2.

Jäggi, A., Bock, H., Thaller, D., et al., 2013. Precise orbit determination of low Earth satellites at AIUB using GPS and SLR data. In: ESA Living Planet Symposium, ESA Special Publications 722, 06 Sep.-13 Sep. 2013, Edinburgh, United Kingdom.

Jäggi, A., Dahle, C., Arnold, D., et al., 2016. Swarm kinematic orbits and gravity fields from 18 months of GPS data. Adv. Space Res. 57(1):218–233. doi:10.1016/j.asr.2015.10.035.

Johnston, G., Riddell, A., Hausler, G., 2017. The International GNSS Service. In Teunissen, Peter J.G., Montenbruck, O. (Eds.), Springer Handbook of Global Navigation Satellite Systems (1st ed., pp. 967-982). Cham, Switzerland: Springer International Publishing. doi:10.1007/978-3-319-42928-1.

Kobel, C., Arnold, D., and Jäggi, A., 2019. Combination of precise orbit solutions for Sentinel-3A using Variance Component Estimation. Adv. in Geosci. 50:27–37. doi:10.5194/adgeo-50-27-2019.

Loyer, S., Perosanz, F., Mercier, F., et al., 2012. Zero-difference GPS ambiguity resolution at CNES-CLS IGS Analysis Center. J. Geod. 86(11):991—1003. doi:10.1007/s00190-012-0559-2.

Lyard, F., Lefevre, F., Letellier, T., et al., 2006. Modelling the global ocean tides: modern insights from FES2004. Ocean Dynam. 56:394–415. doi:10.1007/s10236-006-0086-x.

Mao, X., Visser, P.N.A.M., and Van den IJssel, J., 2018. The impact of GPS receiver modifications and ionospheric activity on Swarm baseline determination. Acta Astronaut. 146:399–408. doi:10.1016/j.actaastro.2018.03.009.

Mao, X., 2019a. Absolute and relative orbit determination for satellite constellations. PhD thesis, Delft University of Technology, ISBN:978-94-028-1555-9.

Mao, X., Visser, P.N.A.M., and Van den IJssel, J., 2019b. High-dynamic baseline determination for the Swarm constellation. Aerosp. Sci. Technol. 88:329–339. doi:10.1016/j.ast.2019.03.031.

Mayer-Gürr, T., Pail, R., Fecher, R., and GOCO Team, 2015. Mayer-Gürr, T and Pail, R and Fecher, R and GOCO Team. In: European Geosciences Union General Assembly 2015, 12 Apr.-17 Apr., 2015, Vienna, Austria.

Molina, J., Peter, H., Fernández, J., et al., 2019. Copernicus Sentinel–3B–GPS L2C tracking tests during commissioning phase. Adv. Space Res, in press, doi:10.1016/j.asr.2019.11.017.

Montenbruck, O., Garcia-Fernandez, M., Yoon, Y., et al., 2009. Antenna phase center calibration for precise positioning of LEO satellites. GPS Solu. 13(1):23–34. doi:10.1007/s10291-008-0094-z.

Montenbruck, O., and Gill, E., 2012. Satellite orbits: models, methods and applications. Springer Science & Business Media, ISBN10:3642583512, ISBN13:9783642583513.

Montenbruck, O., Hackel, S., and Jäggi, A., 2018a. Precise orbit determination of the Sentinel-3A altimetry satellite using ambiguity-fixed GPS carrier phase observations. J. Geod. 92:711–726. doi:10.1007/s00190-017-1090-2.

Montenbruck, O., Hackel, S., Van den IJssel, J., et al., 2018b. Reduced dynamic and kinematic precise orbit determination for the Swarm mission from 4 years of GPS tracking. GPS Solut. 22(79):1–11. doi:10.1007/s10291-018-0746-6.

Pearlman, M.R., Degnan, J.J., and Bosworth, J.M., 2002. The international laser ranging service. Adv. Space Res. 30 (2): 135-143. doi:10.1016/S0273-1177(02)00277-6.

Pesnell, W., 2016. Predictions of solar cycle 24: How are we doing? Space Weather 14(1):10–21. doi:10.1002/2015SW001304.

Peter, H., Jäggi, A., Fernández, J., et al., 2017. Sentinel-1A–First precise orbit determination results. Adv. Space Res. 60(5):879–892. doi:10.1016/j.asr.2017.05.034.

Peter, H., Fernández, J., and Femenias, P., 2020. Copernicus Sentinel-1 satellites: sensitivity of antenna offset estimation to orbit and observation modelling. Adv. Geosci. 50:87–100. doi:10.5194/adgeo-50-87-20204.

Picone, J.M., Hedin, A.E., Drob, D.P., et al., 2002. NRLMSISE-00 empirical model of the atmosphere: statistical comparisons and scientific issues. J. Geophys. Res. Space Phys. 107(A12):SIA–15. doi:10.1029/2002JA009430.

Pilinski, M.D., Argrow, B.M., Palo, S.E., et al., 2013. Semi-empirical satellite accommodation model for spherical and randomly tumbling objects. J. of Spacecr. Rockets 50(3):556–571. doi:10.2514/1.A32348.

Ray, R.D., and Ponte, R.M., 2003. Barometric tides from ECMWF operational analyses. Ann. Geophys. 2003(21): 1897–1910. doi:10.5194/angeo-21-1897-2003.

Ries, J.C., Shum, C.K., and Tapley, B.D., 1993. Surface force modeling for precision orbit determination. Washington DC American Geophysical Union Geophysical Monograph Series 73:111-124. doi:10.1029/GM073p0111.

Savcenko, R., and Bosch, W., 2012. EOT11A-empirical ocean tide model from multi-mission satellite altimetry. Technical Report, Deutsches Geodätisches Forschungsinstitut No. 89.

Schaer, S., Villiger, A., Arnold, D., et al, 2020. The CODE ambiguity-fixed clock and phase bias analysis products: generation, properties and performance. J. Geod. Submitted.

Schmid, R., Dach, R., Collilieux, X., et al., 2016. Absolute IGS antenna phase center model igs08.atx: status and potential improvements. J. Geod. 90(4):343–364. doi:10.1007/s00190-015-0876-3.

Schreiter, L.F., Arnold, D., Sterken, V.J., et al., 2019. Mitigation of ionospheric signatures in Swarm GPS gravity field estimation using weighting strategies, in: Ann. Geophys., Copernicus Publications. pp:111–127. doi:10.5194/angeo-37-111-2019.

Siemes, C., 2020. Swarm satellite thermo-optical properties and external geometry, ESA-EOPG-MOM-MO-15, Revision 2.1, Approved on 2020/4/22. Technical Report. European Space Agency, url: https://earth.esa.int/documents/10174/2563139/Swarm_thermo-optical_properties_and_external_geometry.p (last accessed: 12 Sep., 2020)

Standish, E.M., Williams, J.G., et al., 1992. Orbital ephemerides of the Sun, Moon, and planets. Explanatory supplement to the astronomical almanac, pp:279–323.

Teixeira da Encarnação, J., Visser, P., Arnold, D., et al., 2020. Description of the multi-approach gravity field models from Swarm GPS data. Earth Syst. Sci. Data Discuss. 12(2):1385–1417. doi:10.5194/essd-12-1385-2020.

Van den IJssel, J., Encarnação, J., Doornbos, E., et al., 2015. Precise science orbits for the Swarm satellite constellation. Adv. Space Res. 56(6):1042–1055. doi:10.1016/j.asr.2015.06.002.

Van den IJssel, J., Forte, B., and Montenbruck, O., 2016. Impact of Swarm GPS receiver updates on POD performance. Earth Planets Space 68(85):1–17. doi:10.1186/s40623-016-0459-4.

Van den IJssel, J., Doornbos, E., Iorfida, E., et al., 2020. Thermosphere densities derived from Swarm GPS observations. Adv. Space Res. 65(7):1758-1771. doi:10.1016/j.asr.2020.01.004.

Vielberg, K., Kusche, J., 2020. Extended forward and inverse modeling of radiation pressure accelerations for LEO satellites. J. Geod. 94:art.43. doi:10.1007/s00190-020-01368-6.

Visser, P., Van den IJssel, J., Van Helleputte, T., et al., 2009. Orbit determination for the GOCE satellite. Adv. Space Res. 5(43):760–768. doi:10.1016/j.asr.2008.09.016.

Wermuth, M., Montenbruck, O., Van Helleputte, T., 2010. GPS high precision orbit determination software tools (GHOST), in: Proceedings of 4th International Conference on Astrodynamics Tools and Techniques, pp:3–6, 03 May-06 May, 2010, Madrid, ESA WPP-308.

Wielicki, B.A., Barkstrom, B.R., Harrison, E.F., et al., 1996. Clouds and the Earth's radiant energy system (CERES): An Earth observing system experiment. Bulletin of the American Meteorological Society 77, 853–868.

Yunck, T.P., 1996. Orbit determination. Prog. Astronaut. Aeronaut. 164:559–592. doi:10.2514/5.9781600866395.0559.0592.